

Nature of Ideal MHD instabilities as described by Multi-Region relaxed MHD

A. Kumar,^{1, a)} C. Nührenberg,² Z. Qu,¹ M. J. Hole,^{1,3} J. Doak,¹ R. L. Dewar,¹ S. R. Hudson,⁴ J. Loizu,⁵ K. Aleynikova,² A. Baillod,⁵ and H. Hezaveh¹

¹⁾*Mathematical Sciences Institute, The Australian National University (ANU), Canberra, ACT 2001, Australia*

²⁾*Max-Planck-Institut für Plasmaphysik, IPP-Euratom Association, Teilinstitut Greifswald, 17491 Greifswald, Germany*

³⁾*Australian Nuclear Science and Technology Organisation (ANSTO), Locked Bag 2001, Kirrawee DC NSW 2232, Australia*

⁴⁾*Princeton Plasma Physics Laboratory (PPPL), Princeton University, PO Box-415, New Jersey 08453, United States of America*

⁵⁾*École Polytechnique Fédérale de Lausanne (EPFL), Swiss Plasma Center, CH-1015 Lausanne, Switzerland*

(Dated: 28 April 2022)

In the following work, the Stepped Pressure Equilibrium Code (SPEC) [Hudson, Dewar *et al.*, *Phys. Plasmas* 19, 112502 (2012)] which computes the equilibria of Multi-Region relaxed Magnetohydrodynamic energy principle (MRxMHD), has been upgraded to determine the MRxMHD stability in toroidal geometry. A theoretical formalism for SPEC is obtained by relating the second variation of the MRxMHD energy functional to the Hessian matrix, enabling the prediction of MHD linear instabilities. Negative eigenvalues of this matrix imply instability. Further, we demonstrate our method on simplified test scenarios in both tokamak and stellarator magnetic topologies, with a systematic comparison study between the marginal stability prediction of the SPEC with the ideal MHD stability code packages CAS3D and MISHKA-1.

I. Introduction

In a toroidal plasma low-frequency plasma modes with wavelengths much greater than the particle Larmor radius can be driven unstable by pressure or current gradients¹. Modes with faster growth rates than the diamagnetic drift frequency², resistive rates, and transport timescales can be described by ideal magnetohydrodynamics (IMHD). The linear MHD stability of such modes is commonly analyzed using a perturbative approach *i.e.* applying an infinitesimal perturbation to an equilibrium state described by

$$(\nabla \times \mathbf{B}) \times \mathbf{B} = \nabla p, \quad (1)$$

$$\nabla \cdot \mathbf{B} = 0, \quad (2)$$

$$\nabla p \neq 0, \quad (3)$$

where \mathbf{B} denotes magnetic field and p denotes an isotropic pressure.³ If $\nabla p = 0$ the IMHD fields are known as force-free fields, with \mathbf{B} satisfying the *Beltrami equation*

$$\nabla \times \mathbf{B} = \mu \mathbf{B}, \quad (4)$$

$$p = \text{const.} \quad (5)$$

The case where μ is not constant with respect to position is sometimes called a nonlinear force-free state⁴, though, as long as μ is independent of \mathbf{B} , the Beltrami equation is a linear elliptic PDE. Conversely, the case where μ is a spatial constant is sometimes called a linear force-free state and the Beltrami equation is also termed the Trkalian equation⁵.

Most toroidal magnetic plasma confinement theory is based on the assumption that \mathbf{B} and p are differentiable, so that the magnetostatic equilibrium is governed by Eqns.1–3, and that the magnetic field is integrable, *i.e.* the field lines lie on continuously nested invariant tori, usually known as flux surfaces. However this continuously nested flux surface assumption is rigorously justified only in “2-D” systems, *i.e.* ones with a continuous symmetry (in particular axisymmetry), but even in a nominally axisymmetric system like a tokamak there may be minor symmetry-breaking perturbations (making the magnetic field “3-D”) that call the assumption of all magnetic field lines lying on such magnetic surfaces into question (see details in^{6,7}).

Furthermore toroidal confinement devices of the stellarator class are designed to break axisymmetry strongly in order to provide poloidal field without strong toroidal current in the plasma. While these devices are designed to have magnetic fields close to integrable, *e.g.* by building in a hidden symmetry^{8,9}, in practice the smoothly nested flux surface assumption is never exactly met.

A consequence is that, on rational flux surfaces with non-zero pressure gradients, the current density \mathbf{j} generally consists of δ -function shielding currents and a potentially non-physical Pfirsch-Schlüter current in the form of a $1/x$ singularity. In IMHD, this occurs as a consequence of enforcing a charge conservation law, $\nabla \cdot \mathbf{j} = 0$, in the presence of a pressure gradient^{10–13}. This means an equilibrium code like the Variational Moments Equilibrium Code (VMEC)¹⁴ based on the assumption of smooth pressure and current profiles can never strictly converge (though they can give a reasonable approximation quickly so VMEC has become the workhorse of stellarator design studies). A number of 3-D equilibrium codes which regularize, in various ways, such singular be-

^{a)}Arunav.Kumar@anu.edu.au

havior implied by IMHD have been written, such as IPEC¹⁵, PIES¹⁶, SIESTA¹⁷, HINT2¹⁸, and GPEC¹⁹.

A different approach to 3-D equilibrium theory is to generalize the relaxation principle that Taylor used successfully to explain magnetic field reversal in turbulent z -pinch experiments by minimizing the total magnetic energy subject to a constant magnetic helicity constraint [for a review see Taylor²⁰]. As Taylor assumed negligible, or at least constant, thermal pressure, his variational principle needs to be generalized to enable modeling of experimental pressure and q profiles in tokamaks and stellarators. The key generalization is the *stepped pressure equilibrium* approach, first introduced by Bruno and Laurence²¹, constructing a weak solution to the IMHD equilibrium by relaxing the continuity of the magnetic field and pressure profiles. By incorporating some aspects of Bruno and Laurence's mathematical framework into a generalized Taylor relaxation principle Hole and Dewar *et.al.*²² introduced Multi-Region Relaxed MHD (MRxMHD) over a decade ago. In MRxMHD, the plasma is partitioned into different Taylor relaxed plasma volumes Ω_l , where each Ω_l is bounded by an ideal interface I_l . These interfaces are taken to be of zero width, since we have assumed a coarse-grained fluid model of the plasma that cannot resolve lengths of the order of a particle gyroradius. MRxMHD also extends Taylor's ideas²⁰, where the plasma in each volume Ω_l will evolve to minimize the magnetic potential and thermal energy under the constraint that the magnetic helicity,

$$K_l = \int_{\Omega_l} d^3\tau \mathbf{A} \cdot (\nabla \times \mathbf{A}), \quad (6)$$

is conserved. In addition to helicity conservation, we also constrain the entropy (related to pressure) in each volume Ω_l . Since we are working in the variation on slow timescales, but short compared with heating and confinement times, we assume the geometric variations to be isentropic. For an ideal gas the entropy S is given in terms of the pressure p and volume V by

$$S = S_0 + \frac{Nk_B}{\gamma - 1} \ln \left(\frac{pV^\gamma}{p_0V_0^\gamma} \right), \quad (7)$$

where S_0 and p_0V_0 are arbitrary reference values, N is the number of particles, k_B is Boltzmann's constant, and γ is the ratio of the specific heat capacities. Thus the constancy of N and S implies the well-known adiabatic isentropic ideal-gas constraint

$$pV^\gamma = p_0V_0 \exp\left(\left(\gamma-1\right)\frac{S-S_0}{Nk_B}\right) = \text{const.} \quad (8)$$

We assume Eqn.(8) applies to both the ion and electron gases as a single fluid, so the total pressure $p \equiv p_i + p_e$ also obeys $pV^\gamma = \alpha_l = \text{const.}$ In MRxMHD, these constraints are augmented as non-holonomic constraints with respect to a given reference frame, and are stated in Dewar *et.al.*²³.

The theory of MRxMHD allows for a much less-restrictive class of variations as compared to IMHD, the variations that allow the magnetic field to form magnetic islands and magnetic field-line chaos. Hence, based on the set of non-

holonomic constraints, the variational form of MRxMHD energy functional is written as²⁴

$$F = \sum_{l=1}^{N_v} \left[U_l - \frac{1}{2} \mu_l (K_l - K_{l,0}) \right], \quad (9)$$

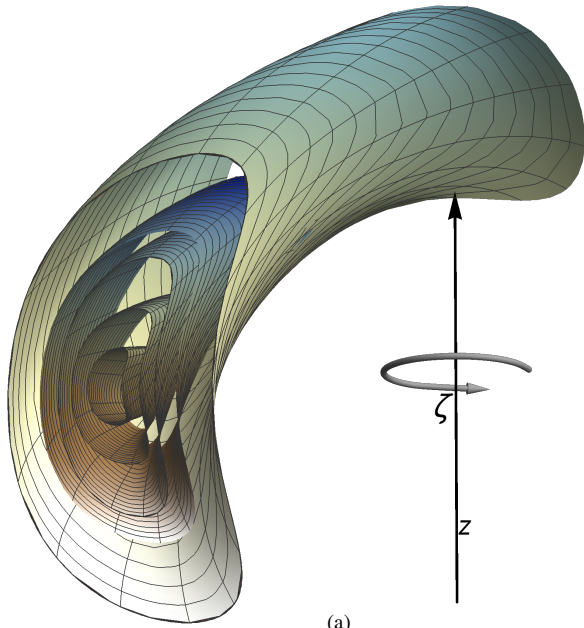
where

$$U_l = \int_{\Omega_l} d^3\tau \left(\frac{p}{\gamma-1} + \frac{B^2}{2} \right), \quad (10)$$

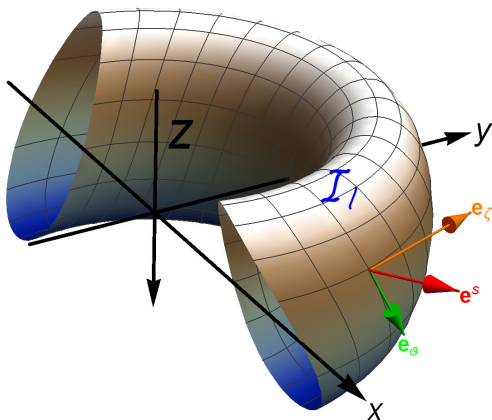
in which μ_l is the Lagrange multiplier, the term U_l is the magnetic potential energy, and N_v is the number of volumes. The plasma volumes Ω_l are enclosed by ideal interfaces, and are constrained to have helicity $K_{l,0}$, $\Delta\psi_{p,l}$ the poloidal flux, and $\Delta\psi_{t,l}$ the toroidal flux. Figure 1a and 1b provides a sketch of an MRxMHD description with $N_v = 5$ regions, and the description of tangential basis vectors on an interface, I_l , respectively.

Because there is no minimum scale length in zero-Larmor-radius MHD, the full solution space includes singular structures such as the discontinuities in p and \mathbf{B} . Thus, rather than the pointwise-defined solutions of classical ideal MHD analysis, MRxMHD seeks the weak solutions defined in the context of normed function spaces²⁴. The weak solutions or the Euler-Lagrange equations for the extremizing states of MRxMHD are as follows. In each volume Ω_l , setting the first variation of the MRxMHD energy functional resulting from variations in the vector potential, \mathbf{A} , to zero leads to the Beltrami equation, $\nabla \times \mathbf{B} = \mu_l \mathbf{B}$, and thus indicates the pressure, $p = \text{const.}$ in each volume Ω_l . In addition, the ideal interfaces I_l with infinite conductance, are required to satisfy the tangential boundary condition $\mathbf{B} \cdot \mathbf{n} = 0$, where \mathbf{n} denotes the outward pointing normal vector to the surfaces. The variations of interface geometry I_l satisfies a pressure balance across the interfaces, given as $\left[\left[p + \frac{B^2}{2} \right] \right]_l = 0$. The $[[\cdot]]_l$ denotes the discontinuity across the l^{th} interface. The pressure profile is thus piecewise constant or a stepped function.

To compute the extremizing states of MRxMHD energy principle, the Stepped-Pressure Equilibrium Code (SPEC)²⁴ was developed, and for a decade now it has been broadly utilized within the stellarator community. In the tokamak community, thus far most the SPEC applications have been theoretical, by which the authors mean in simplified tokamak geometry with the goal of better understanding some theoretical aspects of 3D equilibria, such as the formation of singular currents and saturated tearing modes. In recent years, SPEC has been used in theoretical physics studies, such as the symmetry breaking of quasi-helical states in Reverse Field Pinches (RFP)²⁵, the response of resonant magnetic pressure amplification²⁶, an existence criterion for 3D current sheets²⁷, beta limits in classical stellarator^{28,29}, linear stability and non-linear saturation of tearing modes in slab geometry^{30,31}, free-boundary tokamak equilibria³². In addition, the theory of MRxMHD also been extended to include the effects of pressure anisotropy³³, the two-fluids³⁴, the compressible Euler-fluid and Beltrami field spectrum³⁵, the cross-field flow using phase-space action³⁶ and the self-consistent dynamics of its current sheets^{23,37}.



(a)



(b)

FIG. 1: (a) Pictorial view of nested plasma regions, P_l , separated by toroidal interfaces, I_l (coloured thin sheets), and a plasma boundary (coloured in light green) in MRxMHD; (b) covariant basis vectors \mathbf{e}_θ and \mathbf{e}_ζ (not to scale) and the normal basis vector $\mathbf{e}^s = \nabla s$ to an interface, I_l . The arbitrary toroidal angle, ζ as indicated, is used in the curvilinear coordinate representation.

In the context of the stability studies of hydro-magnetic plasmas, Kruskal *et al.*^{38,39} and Greene *et al.*⁴⁰ discussed a second-order expression of an energy principle known as the second variation. In mathematical terminology, the Taylor ex-

pansion of F in a small parameter ε must be of the form

$$\begin{aligned} \mu_0 F = & F_0 + \varepsilon \sum_{l=1}^{N_v-1} \left(\xi_l \cdot \frac{\delta F}{\delta \xi_l} \right), \\ & + \frac{\varepsilon^2}{2} \sum_{l,l'=1}^{N_v-1} \left(\xi_l^T \cdot \frac{\delta^2 F}{\delta \xi_l \delta \xi_{l'}} \cdot \xi_{l'} \right), \\ & + \dots, \end{aligned} \quad (11)$$

where ξ_l , $\xi_{l'}$ denotes the linear perturbation to interfaces. Here, note that we assume F has been minimized, under the constraints (magnetic helicity and ideal gas law), with respect to the p and \mathbf{A} in each region and they have been eliminated as independent variables. That is, p and the \mathbf{A} are function of the shapes of the interfaces I_l , and so as F . These are infinite-dimensional generalizations of the gradient vector and Hessian matrix, respectively, but will in practice be made finite dimensional by expanding the ξ_l and $\xi_{l'}$ in finite basis sets. In recent investigations of linear MRxMHD stability in pressureless cylindrical⁴¹ and slab³¹ plasma, the Hessian algorithm which is often defined as the second variation of energy functional F , was developed for SPEC.

In recent years, various 3D equilibrium investigations of MRxMHD have been carried out in practice. As such, the understanding of the pressure-driven linear instabilities in terms of multi-region relaxed equilibria have not been explored much, and yet are crucial for 3D MHD stability. Another motivation behind assessing MRxMHD stability using SPEC is the stellarator optimization. In spite of the fact that, the insights and optimization tools used to design present stellarator experiments like Helically Symmetric Experiment⁴² and Wendelstein (W7-X)⁴³ were effective, there are areas in which our understanding of the mathematical principles, the 3D numerical codes and the optimization procedures can be essentially investigated. In specific, optimizing for next generation conceivable stellarator reactors require hundreds and thousands of numerical iterations. Subsequently, the computation of the linear 3D MHD stability and equilibrium simultaneously would be quite sufficient (or, to some degree worthy) for optimisation purposes since they are, first of all, fast and give us a necessary information about possible destabilisation of some modes.

To address such equilibrium and stability calculations in detail, this article demonstrates the extension of the theoretical description of global MHD stability of MRxMHD in toroidal geometry, as well as the derivation of the stability matrix, which contains the second variation of the MRxMHD energy functional F known as the ‘‘Hessian matrix’’ for SPEC, while accounting for adiabatic pressure change. Our derivation is general, as it does not consider the assumption of axisymmetry, and has the potential to interpret the stability conditions in terms of energy consideration for 2D (tokamak) and 3D (stellarator) magnetic geometries.

In this article, the authors aim to present the foundations for numerical studies of MRxMHD/SPEC stability in toroidal geometries, which are described in following points:

- (a) First and foremost, we address some aspects of MRxMHD stability in circular-cross-section tokamaks,

specifically the two sub-classes of pressure-gradient driven MHD instabilities in tokamak plasmas, namely the ideal internal kink and low- n shear ballooning modes.

- (b) Secondly, we use SPEC to investigate the global MRxMHD instabilities in a five field period stellarator configuration. The computational investigations reported here will aid in the clarification of structural properties of global, ideal-MHD-like modes of MRxMHD plasmas, which will be compared with the results from CAS3D, an ideal MHD stability code package.

Furthermore, we present conclusive numerical arguments and observations addressing whether MRxMHD can reveal pressure-gradient driven instabilities.

To our knowledge, the requisite time-dependent non-linear MHD codes are also under development (NIMROD^{44,45}, MEGA⁴⁶, and M3D-C1^{47,48}), and have been extended to treat stellarator geometry. The JOREK^{49,50} code is also developing stellarator functionality based on reduced MHD. In the future, it may also be possible to apply the codes mentioned above in stellarator optimisations.

Recently SPEC has undergone significant up-grades⁵¹. Zernike polynomials have been employed as the radial basis functions, which allows us to calculate well resolved SPEC equilibria at required computational accuracy. SPEC is based on a hybrid spectral-Galerkin representation. So, it may be argued that the scale of our generalised stability matrix, which will be detailed later, could be huge at larger n and m Fourier harmonics. This is well addressed by the shared-memory MPI parallelization. At present, the SPEC Stability has been parallelized with MPI in a similar fashion to the equilibrium construction. That is, each volume is associated with one central processing unit (CPU); since the solution to the perturbed magnetic field in a volume is independent from other volumes, each CPU can solve the coupled linear system in parallel (will be discussed in Section III B.). Finally, the master CPU gathers all required derivatives to construct the stability matrix and solves the linear system, before broadcasting the values to all CPUs.

This article is structured as follows. Section II outlines and reviews the numerical description to compute an extremum of MRxMHD equilibrium with SPEC. In Section III A we describe and elaborate the coordinate-independent theory behind the MRxMHD stability in Eulerian variations, and III B derives generalized stability matrix also known as the Hessian matrix with respect to SPEC co-ordinate system, for numerical implementation. In addition, we also state the *sufficient* and *necessary* conditions of MRxMHD stability. In Section IV, we provide a detailed comparison study of marginal stability prediction of SPEC Stability with the ideal MHD stability codes, and highlight the significance of MRxMHD energy principle to predict the pressure-gradient driven MHD instabilities. Finally, in Section V we briefly summarize our conclusion and discuss future work.

II. Description of SPEC co-ordinate system and discretized form of MRxMHD energy functional

For simplicity, we restrict our attention to fields with stellarator symmetry⁵² which implies

$$R_l(-\vartheta, -\zeta) = R_l(\vartheta, \zeta), \quad (12)$$

$$Z_l(-\vartheta, -\zeta) = -Z_l(\vartheta, \zeta). \quad (13)$$

In SPEC, an interface I_l is described with

$$\mathbf{x}_l(\vartheta, \zeta) = R_l(\vartheta, \zeta)\hat{\mathbf{e}}_R + Z_l(\vartheta, \zeta)\hat{\mathbf{e}}_Z. \quad (14)$$

Here, $\hat{\mathbf{e}}_R = \cos\phi\hat{i} + \sin\phi\hat{j}$ for the toroidal angle $\zeta = \phi$, and the $R_l(\vartheta, \zeta)$ and $Z_l(\vartheta, \zeta)$ are an even and odd function of (ϑ, ζ) respectively. The symmetric and non-symmetric variables are discretised in the Fourier basis function as

$$R_l(\vartheta, \zeta) = \sum_{m,n} R_{l,m,n} \cos(m\vartheta - nN_f\zeta), \quad (15)$$

$$Z_l(\vartheta, \zeta) = \sum_{m,n} Z_{l,m,n} \sin(m\vartheta - nN_f\zeta). \quad (16)$$

The set of parameters $\{R_{l,m,n}, Z_{l,m,n} \in \mathbb{R}^2, (m,n) \in (\mathbb{N}^* \times \mathbb{Z}) \cup (\{0\} \times \mathbb{N})\}$ uniquely defines the shapes of the interfaces. The number of field periods, $N_f \in \mathbb{N}^*$ represents the discrete rotational symmetry of an equilibrium. For an annular volume Ω_l which is enclosed by the adjacent interfaces \mathbf{x}_{l-1} and \mathbf{x}_l , the co-ordinate functions are described using a linear interpolation, given by

$$R(s, \vartheta, \zeta) = \sum_{m,n} \left[\frac{1-s}{2} R_{l-1,m,n} + \frac{1+s}{2} R_{l,m,n} \right] \times \cos(m\vartheta - nN_f\zeta), \quad (17)$$

$$Z(s, \vartheta, \zeta) = \sum_{m,n} \left[\frac{1-s}{2} Z_{l-1,m,n} + \frac{1+s}{2} Z_{l,m,n} \right] \times \sin(m\vartheta - nN_f\zeta), \quad (18)$$

where $s \in [-1, 1]$ is regarded as local radial co-ordinate.

In SPEC²⁴, the equilibrium magnetic field \mathbf{B} is given by the vector potential \mathbf{A} which takes the Clebsch form as $\mathbf{A} = A_\vartheta(s, \vartheta, \zeta)\nabla\vartheta + A_\zeta(s, \vartheta, \zeta)\nabla\zeta$ in the Eulerian reference frame. In each volume Ω_l , the components of vector potentials are written in the Fourier-Zernike basis representation,

$$A_\vartheta(s, \vartheta, \zeta) = \sum_{m \geq 0, n, z=m}^{L_M} A_{\vartheta,m,n,l} \bar{P}_z^m(s) \cos(m\vartheta - nN_f\zeta) \quad (19)$$

$$A_\zeta(s, \vartheta, \zeta) = \sum_{m \geq 0, n, z=m}^{L_M} A_{\zeta,m,n,l} \bar{P}_z^m(s) \cos(m\vartheta - nN_f\zeta) \quad (20)$$

where $A_{\vartheta,m,n,l}, A_{\zeta,m,n,l}$ are the Fourier-Zernike coefficients and L_M is related to the highest resolution of Zernike polynomial $\bar{P}_z^m(s)$, and s is a radial coordinate. Here, the $\bar{P}_z^m(s)$ is scaled as $P_z^m(s)/1+z$ for $m \geq 2$. For poloidal mode harmonics $m = 0$ and $m = 1$, a basis recombination of Zernike polynomial is employed to mitigate the co-ordinate singularity³² in the innermost volume of the plasma domain. Subtleties are stated in Qu *et al.*⁵¹.

The magnetic field is then represented in contravariant form as, $\sqrt{g}\mathbf{B} = \sqrt{g}B^s\mathbf{e}_s + \sqrt{g}B^\vartheta\mathbf{e}_\vartheta + \sqrt{g}B^\zeta\mathbf{e}_\zeta$ where these contravariant coefficients are written in terms of coefficients of vector potential,

$$\sqrt{g}B^s = \sum_{m \geq 0, n, z=m}^{L_M} (mA_{\vartheta, m, n, l} - nN_f A_{\zeta, m, n, l}) \bar{P}_z^m(s) \quad (21)$$

$$\times \sin(m\vartheta - nN_f\zeta),$$

$$\sqrt{g}B^\vartheta = - \sum_{m \geq 0, n, z=m}^{L_M} A_{\zeta, m, n, l} \bar{P}_z^m(s) \cos(m\vartheta - nN_f\zeta), \quad (22)$$

$$\sqrt{g}B^\zeta = \sum_{m \geq 0, n, z=m}^{L_M} A_{\vartheta, m, n, l} \bar{P}_z^m(s) \cos(m\vartheta - nN_f\zeta), \quad (23)$$

where the primes denotes the derivative of $\bar{P}_z^m(s)$ with respect to s and the Jacobian is described as

$$\sqrt{g} = (\nabla s \times \nabla \vartheta \cdot \nabla \zeta)^{-1}, \quad (24)$$

under the toroidal co-ordinate system $(s, \vartheta, \zeta) \in [-1, 1] \times [0, 2\pi) \times [0, 2\pi)$ where $s = -1$ and $s = 1$ are the notation for inner and outer interface, respectively. Hence, here s is a local radial variable.

In each volume Ω_l of SPEC, the constrained energy functional F_l depends on the vector potential \mathbf{A} , and the Lagrange multipliers $\mu_l, c_1, d_1, a_{m,n}, b_{m,n}, e_{m,n}$, and takes the form

$$F_l \equiv \frac{1}{2} \int_{\Omega_l} B^2 \sqrt{g} d\vartheta d\zeta ds + \int_{\Omega_l} \frac{\mu_0 p}{\gamma - 1} \sqrt{g} d\vartheta d\zeta ds, \quad (25)$$

$$- \frac{\mu_l}{2} \left(\int_{\Omega_l} \mathbf{A} \cdot \mathbf{B} \sqrt{g} d\vartheta d\zeta ds - K_{l,0} \right),$$

$$+ c_l \left(\oint_{C_{p,l}^<} \mathbf{A} \cdot \mathbf{e}_\vartheta d\vartheta - \Delta\psi_{t,l} \right),$$

$$+ d_l \left(\oint_{C_{t,l}^>} \mathbf{A} \cdot \mathbf{e}_\zeta d\zeta - \Delta\psi_{p,l} \right),$$

$$+ \sum_{m,n} e_{m,n} \iint_{\partial\Omega_l} \sqrt{g}\mathbf{B} \cdot \nabla s \cos(m\vartheta - nN_f\zeta) d\vartheta d\zeta,$$

$$+ \sum_{m,n} a_{m,n} \sum_{z=m}^{L_M} A_{\vartheta, m, n, l} \bar{P}_z^m(-1),$$

$$+ \sum_{m,n} b_{m,n} \sum_{z=m}^{L_M} A_{\zeta, m, n, l} \bar{P}_z^m(-1),$$

where the $C_{p,l}^<$ and $C_{t,l}^>$ are circuits about the inner ($<$) and outer ($>$) boundaries of Ω_l in the poloidal and toroidal directions respectively. The enclosed poloidal flux $\Delta\psi_{p,l}$, toroidal flux $\Delta\psi_{t,l}$ and the interface boundary condition $\sqrt{g}\mathbf{B} \cdot \nabla s = 0$ are enforced by a set of Lagrange multipliers (e_i for the i^{th} Fourier harmonic of interface boundary condition, and c_l, d_l for fluxes)³². Additionally, in annular volumes, the gauge freedom of vector potential defined as $A_\vartheta(-1, \vartheta, \zeta) = 0$ and $A_\zeta(-1, \vartheta, \zeta) = 0$ are enforced by the Lagrange multipliers a_i and b_i respectively for the i^{th} Fourier harmonics. The discussion on gauge dependency and interface boundary condition can be found in Hudson *et al.*²⁴.

By denoting $\mathbf{a} \equiv \{A_{\vartheta, m, n, l}, A_{\zeta, m, n, l}, a_{m,n}, b_{m,n}, e_{m,n}, c_l, d_l\}$ and $\boldsymbol{\psi} \equiv \{\Delta\psi_{t,l}, \Delta\psi_{p,l}\}$, the discretized energy functional $F_l(\mathbf{x}_l, \mathbf{a}, \mu_l)$ within each SPEC volume Ω_l can be written as

$$F_l = \frac{1}{2} \mathbf{a}^T \cdot \mathcal{A}_l(\mathbf{x}_l) \cdot \mathbf{a} - \mu_l \frac{1}{2} (\mathbf{a}^T \cdot \mathcal{D}_l \cdot \mathbf{a} - K_{l,0}) - \mathbf{a}^T \cdot \mathcal{B}_l \cdot \boldsymbol{\psi}. \quad (26)$$

The matrices $\mathcal{A}_l, \mathcal{B}_l$ and \mathcal{D}_l are constructed in each Ω_l by inserting the representation for the vector potential given in Eqn.(19) and (20) into Eqn.(25) and computing the volume dependent integrals. The volume integrals are computed with Gauss quadrature and Fast Fourier Transform scheme. We emphasize that the matrix \mathcal{A}_l depends on the geometry of the interfaces \mathbf{x}_l , and also on geometrical metrics and Jacobians. The matrices \mathcal{B}_l and \mathcal{D}_l do not depend upon interface geometry. More detailed construction of elements in these matrices $\mathcal{A}_l, \mathcal{D}_l$ and \mathcal{B}_l are addressed in Hudson *et al.*^{24,32} and Qu *et al.*⁵¹.

The magnetic field that satisfies the Beltrami equation, $\nabla \times \mathbf{B} = \mu_l \mathbf{B}$ in each volume Ω_l is obtained by solving an auxiliary set of equations in each volume Ω_l as

$$\frac{\partial F_l}{\partial \mathbf{a}} = 0, \quad \frac{\partial F_l}{\partial \mu_l} = 0, \quad (27)$$

where F_l is obtained from Eqn.(26). This yields

$$(\mathcal{A}_l - \mu_l \mathcal{D}_l) \cdot \mathbf{a} = -\mathcal{B}_l \cdot \boldsymbol{\psi}, \quad (28a)$$

$$\mathbf{a}^T \cdot \mathcal{D}_l \cdot \mathbf{a} = K_{l,0}. \quad (28b)$$

After computing the Beltrami field in each volume in accordance with the helicity, the flux constraints, and the boundary condition that the field is tangential to the interface, SPEC will then move the position of the interfaces I_l , to force difference on the two sides, $[[p + B^2/2]]_l = 0$ using a nonlinear quasi-Newton iteration. For fixed boundary SPEC equilibrium calculation, SPEC requires the plasma boundary, the enclosed poloidal flux $\Delta\psi_{p,l}$ and toroidal flux $\Delta\psi_{t,l}$, and magnetic helicity $K_{l,0}$ in each volume Ω_l *i.e.* $\{p, \Delta\psi_{p,l}, \Delta\psi_{t,l}, K_{l,0}\}$. In particular, it is also possible to constrain the rotational transform ι on either side of the interfaces such that the equilibrium is described by the $\{p_l, \Delta\psi_{t,l}, \iota^+, \iota^-\}$. This will require an iteration over both $\Delta\psi_{p,l}$ and μ_l for a given toroidal flux $\Delta\psi_{t,l}$ such as to satisfy the ι on either side of the interfaces.

III. Global MRxMHD stability

The aim of this section is to review and elaborate the theoretical derivation of the Eulerian variations for the computational exploration of MRxMHD stability with SPEC.

Before proceeding further, we begin by noting useful generalized transport theorems⁵³ based on the Eulerian variations that we will use in the subsequent derivations. They are

$$\delta \int_{\Omega_l} f d^3 \tau = \int_{\Omega_l} \delta f d^3 \tau + \int_{\partial\Omega_l} (\mathbf{n} \cdot \boldsymbol{\xi}) f d^2 \sigma, \quad (29)$$

$$\delta \int_{\partial\Omega_l} (\mathbf{n} \cdot \vec{f}) d^2 \sigma = \int_{\partial\Omega_l} (\mathbf{n} \cdot \delta \vec{f} + (\mathbf{n} \cdot \boldsymbol{\xi})(\nabla \cdot \vec{f})) d^2 \sigma, \quad (30)$$

where f is the functional under consideration and $\boldsymbol{\xi}$ being the interface displacement.

A. Theory and equations

Owing to the above properties of transport theorems, the second-order variation of the local MRxMHD energy functional $\delta^2 F_l$, accounts for the variations in the vector potential \mathbf{A} , the pressure p , and the interface geometry $\boldsymbol{\xi}$. The second variation yields

$$\begin{aligned} \delta^2 F_l = & \int_{\Omega_l} (\nabla \times \delta \mathbf{B} - \mu_l \delta \mathbf{B}) \cdot \delta \mathbf{A} d^3 \tau, \\ & - \int_{\partial \Omega_l} \boldsymbol{\xi} \cdot \nabla \left(p + \frac{B^2}{2} \right) (\boldsymbol{\xi} \cdot \mathbf{n}) d^2 \sigma, \\ & + \int_{\partial \Omega_l} \delta p \boldsymbol{\xi} \cdot \mathbf{n} d^2 \sigma, \\ & + \int_{\partial \Omega_l} \boldsymbol{\xi} \cdot \left(\left(p + \frac{B^2}{2} \right) (\nabla \cdot \boldsymbol{\xi}) \right) \cdot \mathbf{n} d^2 \sigma, \end{aligned} \quad (31)$$

where $\delta \mathbf{A}$ and δp is the perturbed vector potential and pressure respectively, $\delta \mathbf{B} = \nabla \times \delta \mathbf{A}$, and $\boldsymbol{\xi} \cdot \mathbf{n}$ is the normal component of the displacement of interface I_l . For brevity, we have omitted the equilibrium quantities and their simple algebraic calculation.

To find a more simplified expression, as in Eqn.(51) of Spies *et al.*⁵⁴ we express the vector-algebraic relation as

$$\begin{aligned} & \int_{\Omega_l} (\delta \mathbf{A} \cdot \nabla \times (\nabla \times \delta \mathbf{A}) - |\nabla \times \delta \mathbf{A}|^2) d^3 \tau \\ & = \int_{\partial \Omega_l} (\delta \mathbf{A} \times \mathbf{n}) \cdot (\nabla \times \delta \mathbf{A}) d^2 \sigma. \end{aligned} \quad (32)$$

Further, using Eqn.(32) and the expression for perturbed pressure δp obtained from Eqn.(8) for $\alpha_l = \text{const.}$, the Eqn.(31) can be rewritten as

$$\begin{aligned} \delta^2 F_l = & \int_{\Omega_l} (|\nabla \times \delta \mathbf{A}|^2 - \mu_l \delta \mathbf{A} \cdot (\nabla \times \delta \mathbf{A})) d^3 \tau \\ & + \int_{\partial \Omega_l} ((\delta \mathbf{A} \times \mathbf{n}) \cdot (\nabla \times \delta \mathbf{A})) d^2 \sigma, \\ & - \int_{\partial \Omega_l} \boldsymbol{\xi} \cdot \nabla \left(p + \frac{B^2}{2} \right) (\boldsymbol{\xi} \cdot \mathbf{n}) d^2 \sigma, \\ & - \int_{\partial \Omega_l} \left(\frac{\gamma \alpha_l}{V_l^{\gamma+1}} \delta V_l \right) \boldsymbol{\xi} \cdot \mathbf{n} d^2 \sigma, \\ & + \int_{\Omega_l} \nabla \cdot \left(\boldsymbol{\xi} \left(p + \frac{B^2}{2} \right) (\nabla \cdot \boldsymbol{\xi}) \right) d^3 \tau, \end{aligned} \quad (33)$$

where δV_l is the perturbed volume Ω_l . It is well known, the incompressible plasma limit can be achieved by letting pressure (or more accurately, the acoustic speeds) approach infinity. As a consequence, the Eqn. (33) can also be condensed by taking the MRxMHD in the incompressible limit $\nabla \cdot \boldsymbol{\xi} = 0$, which will be further discussed in Section III A 2.

In more general, on considering the incompressible limit in Dewar *et al.*^{35,37,55} dynamical MRxMHD theories, the ideal interfaces, which act as infinitesimally thin current sheets, supply inertia that specifies the finite frequencies, and only surface waves like the shear-Alfvén wave persist. Thus, it

is incompressibility that imparts inertia to the interfaces, because, when we move an interface, incompressibility forces to move the plasma within the interface, requiring a force on the plasma and an equal and opposite reaction force on the interface. The magneto-sonic acoustic (slow or fast) waves with finite low-frequencies also exist within the Beltrami relaxed sub-regions for compressible MRxMHD plasma⁵⁵, along with coupled surface waves from the interfaces.

1. Derivation of perturbed interface boundary condition

In MRxMHD, when the plasma attains an equilibrium the impermeability of the barrier interfaces to flux implies the local constraint. That is, \mathbf{B} is required to be tangential to an interface I_l on both sides (though \mathbf{B} is not necessarily continuous across I_l as we assume these interfaces can carry current sheets as $\mathbf{j} = \mathbf{n} \times [[\mathbf{B}]]$). Also, the conservation of flux implies the poloidal and toroidal line integral constraints on the interfaces, $\oint_C \mathbf{A} \cdot d\mathbf{l} = \text{const.}$

The tangential condition on boundary surfaces of region Ω_l implies $\nabla_s \cdot \nabla \times \mathbf{A} = 0$. This can be written as

$$\partial_\theta A_\zeta - \partial_\zeta A_\theta = 0 \quad \text{for } \mathbf{r} \in \partial \Omega_l, \quad (34)$$

where \mathbf{r} is defined as the position vector of a general point in plasma such that we represent $s = s(\mathbf{r})$, $\vartheta = \vartheta(\mathbf{r})$ and $\zeta = \zeta(\mathbf{r})$. The general solution for the vector potential \mathbf{A} on $\partial \Omega_l^\pm$ is obtained as

$$A_\vartheta = \partial_\vartheta \chi^\pm, \quad A_\zeta = \partial_\zeta \chi^\pm, \quad (35)$$

where A_s is undetermined, as is the surface potential $\chi^\pm(\vartheta, \zeta)$, which is not single valued and not entirely arbitrary as it responsible for nonzero $\oint_{\partial \Omega_l} \mathbf{A} \cdot d\mathbf{l}$. In coordinate free terms, Eqn.(35) implies $\mathbf{A}_{lgt} = \nabla_{lgt} \chi^\pm$, where the projection of ∇ in the local plane tangent to interface ∇_{lgt} is defined as $(\mathbf{I} - \mathbf{nn}) \cdot \nabla \equiv \mathbf{e}_{lgt}^j \partial_j + \mathbf{e}_{lgt}^k \partial_k$ for $\{i, j, k\}$ being the cyclic triplet. On extending χ^\pm arbitrarily off the surface to define its three-dimensional gradient, this can also be written $\mathbf{n} \times \mathbf{A} = \mathbf{n} \times \nabla \chi^\pm$.

To consider an effect of perturbing the interfaces, we use the transformation

$$\mathbf{r}(s, \vartheta, \zeta, \varepsilon) \equiv \mathbf{R}(s, \vartheta, \zeta | \varepsilon), \quad (36)$$

where ε be the arbitrary perturbation parameter. If we consider ε analogous to dummy time variable, $\boldsymbol{\xi}$ is analogue of a fluid-flow velocity field as $\boldsymbol{\xi}(\mathbf{r}, \varepsilon) \equiv D_\varepsilon \mathbf{r} = \partial \mathbf{R}(s, \vartheta, \zeta | \varepsilon) / \partial \varepsilon$, where D_ε denotes the advective derivative. Since, we are working in the Eulerian frame of reference, we write the advective derivative in terms of Eulerian derivative ∂_ε , as $D_\varepsilon = \partial_\varepsilon + \boldsymbol{\xi} \cdot \nabla$. The fact that $\{\partial_\vartheta, \partial_\zeta\}$ and D_ε commute, taking the advective derivative of Eqn.(34) yields

$$\partial_\vartheta D_\varepsilon A_\zeta - \partial_\zeta D_\varepsilon A_\vartheta = 0 \quad \text{for } \mathbf{r} \in \partial \Omega_l, \quad (37)$$

which is solved on $\partial \Omega_l^\pm$ by [cf. Eqn. (35)]

$$D_\varepsilon A_\vartheta = \partial_\vartheta \chi^\pm, \quad D_\varepsilon A_\zeta = \partial_\zeta \chi^\pm. \quad (38)$$

Here, $\chi^\pm(\vartheta, \zeta|_\varepsilon)$ is a periodic function because of the invariance of the line integrals $\oint_{\partial\Omega_l} \mathbf{A} \cdot d\mathbf{l}$. So, on writing $D_\varepsilon \mathbf{e}^i = -(\nabla \boldsymbol{\xi}) \cdot \mathbf{e}^i$ and taking the advective derivative of contravariant representation of $\mathbf{A} = A_i \mathbf{e}^i$, we find that

$$\partial_\varepsilon \mathbf{A} = (D_\varepsilon A_s) \nabla s + (D_\varepsilon A_\vartheta) \nabla \vartheta + (D_\varepsilon A_\zeta) \nabla \zeta + \boldsymbol{\xi} \times \mathbf{B} - \nabla(\boldsymbol{\xi} \cdot \mathbf{A}). \quad (39)$$

Finally the perturbed boundary condition of \mathbf{A} is obtained by crossing Eqn.(39) with \mathbf{n} and using Eqn.(38)

$$\mathbf{n} \times \partial_\varepsilon \mathbf{A} = -(\mathbf{n} \cdot \boldsymbol{\xi}) \mathbf{B} + \mathbf{n} \times \nabla(\chi^\pm - \boldsymbol{\xi} \cdot \mathbf{A}) \quad \text{for } \mathbf{r} \in \partial\Omega_l^\pm. \quad (40)$$

Therefore, the local solution of the perturbed magnetic field $\delta \mathbf{B}$ within each volume Ω_l is then computed by solving the elliptic partial differential equation along with the simplified form of perturbed boundary condition (Eqn.40), as

$$\nabla \times \delta \mathbf{B} = \mu_l \delta \mathbf{B}, \quad (41a)$$

$$\delta \mathbf{A} \times \mathbf{n} = (\mathbf{n} \cdot \boldsymbol{\xi}) \mathbf{B} + \mathbf{n} \times \nabla(\chi^\pm - \boldsymbol{\xi} \cdot \mathbf{A}). \quad (41b)$$

2. Heuristic characterization of MRxMHD stability equations

When incompressibility is assumed and the pressure variation is minimized to zero, the Eqn.(33) reduces to an interface surface integral of the form

$$\delta^2 F_l = \int_{\partial\Omega_l} (\boldsymbol{\xi} \cdot \mathbf{n}) \mathbf{B} \cdot \delta \mathbf{B} d^2 \sigma - \int_{\partial\Omega_l} \boldsymbol{\xi} \cdot \nabla \left(p + \frac{B^2}{2} \right) (\boldsymbol{\xi} \cdot \mathbf{n}) d^2 \sigma, \quad (42)$$

where $\delta \mathbf{B}$ is the perturbation to the Beltrami field \mathbf{B} , which corresponds to an interface perturbation by a vector field of displacements, $\boldsymbol{\xi} \cdot \mathbf{n}$.

One peculiarity of MRxMHD is the support of non-trivial pressure profiles which retain the force-free fields within each volume. In this article, we have chosen to investigate whether global MRxMHD stability theory supports pressure gradient-driven modes. The argument lies behind the statement of Bernstein *et.al*⁵⁶ that some effort is required to stretch and shift the lines of force if the direction of the magnetic field is changed by the tension *i.e.* an outward force due to the toroidal curvature and the pressure. Thus, in the sense that the ∇B^2 plays an important role, we rewrite the second term of Eqn.(42) as

$$\delta^2 F_l = \int_{\partial\Omega_l} \mathbf{n} \cdot \left\{ \nabla p + ((\mathbf{B} \cdot \nabla) \mathbf{B}) + \mathbf{B} \times (\nabla \times \mathbf{B}) \right\} |\boldsymbol{\xi} \cdot \mathbf{n}|^2 d^2 \sigma, \quad (43)$$

so that we can represent the magnetic curvature with an arbitrary vector radii-of-curvature, \mathbf{C} , from a point on a line of force to the local center of curvature of the interface, as

$$\delta^2 F_l = \int_{\partial\Omega_l} |\boldsymbol{\xi} \cdot \mathbf{n}|^2 \mathbf{n} \cdot \mathbf{C} \frac{B^2}{C^2} d^2 \sigma. \quad (44)$$

This follows from the crucial fact that if \mathbf{C} is directed outward to the plasma, the Eqn.(44) represent the destabilizing effect if $\mathbf{n} \cdot \mathbf{C} < 0$ and an stabilizing effect if $\mathbf{n} \cdot \mathbf{C} > 0$. This is also the main reason behind the ballooning or interchange instability *i.e.* pressure-driven modes which limit the plasma beta, as $\mathbf{n} \cdot \mathbf{C} < 0$. The tension which leads to a force on interfaces is proportional to the curvature of the interfaces *i.e.* $\boldsymbol{\kappa} = \mathbf{C}/C^2 = \mathbf{e}_\parallel \cdot \nabla \mathbf{e}_\parallel$ where $\mathbf{e}_\parallel = \mathbf{B}/B$, and hence this orientation can be separated into the form of normal ($\boldsymbol{\kappa}_\perp$) and the geodesic curvatures ($\boldsymbol{\kappa}_\parallel$). Here, the $\boldsymbol{\kappa}_\parallel = \boldsymbol{\kappa} \cdot (\nabla s \times \mathbf{B})/|B \nabla s|$ where s is flux label, is closely related to the projection of the magnetic field on interfaces onto current flowing parallel within the volume Ω_l (parallel to the magnetic bi-normal direction).

For a quantitative numerical analysis of global stability of MRxMHD, the theory of variational energy principle states that it is *sufficient* and *necessary* to analyze the sign of the second variation of energy for all physical infinitesimal perturbations about an equilibrium state^{30,41}. In the next section we proceed to express the Eqn.(42) in terms of SPEC co-ordinate system to formulate the Hessian. That is, the generalized stability matrix, which is symmetric in nature, as a consequence of the symmetry of second derivatives of the energy functional $F = \sum_l F_l$. Here, F is a smooth function of \mathbf{y} where \mathbf{y} is an arbitrary degrees of freedom. Therefore, for a local or global minimum, $\nabla^2 F$ is positive definite, *i.e.* $\forall \delta \mathbf{y}$, $\delta \mathbf{y}^T \cdot \nabla^2 F \cdot \delta \mathbf{y} > 0$ if $\delta \mathbf{y} \neq \mathbf{0}$. For a saddle point, $\nabla^2 F$ is indefinite, *i.e.* there is some perturbation $\delta \mathbf{y}$ that will lead to a lower energy state, making $\delta \mathbf{y}^T \cdot \nabla^2 F \cdot \delta \mathbf{y} < 0$.

B. Formulation of the Hessian "Generalized stability matrix" for SPEC

Following Ref.⁴¹, we write the Lagrange multiplier μ_l and \mathbf{a}_l to be a function of interface geometry \mathbf{x}_l such that the dependence of $F = \sum_l F_l$ accounts as $F_l \equiv F_l(\mathbf{x}_l, \mathbf{a}_l(\mathbf{x}_l), \mu_l(\mathbf{x}_l))$. In general geometry, the first-order variation to the "local" constrained energy functional $F_l \equiv (U_l - \mu_l/2(K_l - K_{l,0}))$ in each volume Ω_l , yields $\delta F_l = \int_{\Omega_l} (\nabla \times \mathbf{B} - \mu_l \mathbf{B}) \cdot \delta \mathbf{A} d^3 \tau - \int_{\partial\Omega_l} \left(p + \frac{B^2}{2} \right) \boldsymbol{\xi} \cdot d^2 \boldsymbol{\sigma}_s$ where the differential surface area element $d^2 \boldsymbol{\sigma}_s = \sqrt{g} \mathbf{e}^s(s, \vartheta, \zeta) d\vartheta d\zeta$ for constant s labelling of ideal interfaces or the flux surfaces, and $\boldsymbol{\xi} = \delta R_l \hat{\mathbf{e}}_r + \delta Z_l \hat{\mathbf{e}}_z$ denotes the infinitesimal perturbation of interface. On expanding the variational form of δF_l as $\partial F_l / \partial \mathbf{a}_l \cdot \delta \mathbf{a}_l + \partial F_l / \partial \mu_l \cdot \delta \mu_l + \partial F_l / \partial \mathbf{x}_l \cdot \delta \mathbf{x}_l$ as a partial fraction, the first two terms will vanish because of the equilibrium conditions of MRxMHD given in Eqn.(27). The remaining terms can be written as,

$$\delta F_l = - \iint [[p + B^2/2]]_l \boldsymbol{\xi} \cdot \mathbf{n}_l d\vartheta d\zeta, \quad (45)$$

where the normal vector is defined as

$$\begin{aligned} \mathbf{n}_l &= \mathbf{e}_\vartheta \times \mathbf{e}_\zeta, \\ &= R_l Z_{l,\vartheta} \hat{\mathbf{e}}_R + (Z_{l,\vartheta} R_{l,\zeta} - R_{l,\vartheta} Z_{l,\zeta}) \hat{\boldsymbol{\phi}} - R_{l,\vartheta} R_l \hat{\mathbf{e}}_Z, \end{aligned} \quad (46)$$

with covariant basis vectors defined as $\mathbf{e}_\vartheta = R_{l,\vartheta}\hat{\mathbf{e}}_R + Z_{l,\vartheta}\hat{\mathbf{e}}_Z$ and $\mathbf{e}_\zeta = R_{l,\zeta}\hat{\mathbf{e}}_R - R_l\hat{\boldsymbol{\phi}} + Z_{l,\zeta}\hat{\mathbf{e}}_Z$.

To find an expression for the Hessian matrix, we express Eqn.(45) using Eqn.(14) in terms of the Fourier-Poisson summation, which yields

$$\frac{\partial F_l}{\partial R_{l,m,n}} = - \sum_{\tilde{m}, \tilde{n}} \sum_{\tilde{m}, \tilde{n}} \sum_{\tilde{m}, \tilde{n}} \sum_{\tilde{m}, \tilde{n}} \left[\left[p + \frac{B^2}{2} \right] \right]_{l, \tilde{m}, \tilde{n}} \tilde{m} R_{l, \tilde{m}, \tilde{n}} Z_{l, \tilde{m}, \tilde{n}} \quad (47)$$

$$\times I_{m,n, \tilde{m}, \tilde{n}, \tilde{m}, \tilde{n}, \tilde{m}, \tilde{n}},$$

$$\frac{\partial F_l}{\partial Z_{l,m,n}} = + \sum_{\tilde{m}, \tilde{n}} \sum_{\tilde{m}, \tilde{n}} \sum_{\tilde{m}, \tilde{n}} \sum_{\tilde{m}, \tilde{n}} \left[\left[p + \frac{B^2}{2} \right] \right]_{l, \tilde{m}, \tilde{n}} R_{l, \tilde{m}, \tilde{n}} R_{l, \tilde{m}, \tilde{n}} \quad (48)$$

$$\times (-\tilde{m}) J_{m,n, \tilde{m}, \tilde{n}, \tilde{m}, \tilde{n}, \tilde{m}, \tilde{n}},$$

where

$$I_{m,n, \tilde{m}, \tilde{n}, \tilde{m}, \tilde{n}, \tilde{m}, \tilde{n}} = \oint \oint \cos(\tilde{\alpha}) \cos(\tilde{\alpha}) \cos(\alpha) \quad (49)$$

$$\times \cos(\tilde{\alpha}) d\vartheta d\zeta,$$

$$J_{m,n, \tilde{m}, \tilde{n}, \tilde{m}, \tilde{n}, \tilde{m}, \tilde{n}} = \oint \oint \sin(\tilde{\alpha}) \cos(\tilde{\alpha}) \sin(\alpha) \quad (50)$$

$$\times \sin(\tilde{\alpha}) d\vartheta d\zeta,$$

are the integral over even functions with $\tilde{\alpha} = \tilde{m}\vartheta - \tilde{n}N_f\zeta$, $\tilde{\alpha} = \tilde{m}\vartheta - \tilde{n}N_f\zeta$, and $\alpha = m\vartheta - nN_f\zeta$, $\tilde{\alpha} = \tilde{m}\vartheta - \tilde{n}N_f\zeta$ and $[[\dots]]$ denotes the pressure-jump discontinuity term. From Sec.II, B^2 is defined in contravariant form *i.e.* $B^2 = (B^\vartheta B^\vartheta g_{\vartheta\vartheta} + 2B^\vartheta B^\zeta g_{\vartheta\zeta} + B^\zeta B^\zeta g_{\zeta\zeta})$ where the lower metric coefficients $g_{i,j}$'s are

$$g_{\vartheta\vartheta} = \mathbf{e}_\vartheta \cdot \mathbf{e}_\vartheta = R_{l,\vartheta}R_{l,\vartheta} + Z_{l,\vartheta}Z_{l,\vartheta}, \quad (51a)$$

$$g_{\vartheta\zeta} = \mathbf{e}_\vartheta \cdot \mathbf{e}_\zeta = R_{l,\vartheta}R_{l,\zeta} + Z_{l,\vartheta}Z_{l,\zeta}, \quad (51b)$$

$$g_{\zeta\zeta} = \mathbf{e}_\zeta \cdot \mathbf{e}_\zeta + R^2 = R_{l,\zeta}R_{l,\zeta} + Z_{l,\zeta}Z_{l,\zeta} + R^2. \quad (51c)$$

By construction, the contravariant component $B^\vartheta = 0$ on the ideal interfaces. Also we remark that here the B^2 is a function of interface geometry \mathbf{x}_l , and so are the Jacobian \sqrt{g} and the lower metric coefficients g_{ij} 's.

Following the theories of III A, the stability of an MRxMHD equilibrium can be accessed by the change in the $\delta F / \delta \mathbf{x}_l$ for an infinitesimal geometrical deformation of the interfaces, and this form of change is numerically interpreted as the Hessian matrix,

$$\mathbf{H}_{j,k,l,l'} = \frac{\delta}{\delta \mathbf{x}_{l',k}} (\delta F_l / \delta \mathbf{x}_{l,j}), \quad (52)$$

where $j = (m_j, n_j)$ and $k = (m_k, n_k)$ are defined as dummy set of variable for the Fourier harmonics for clarity, with $N_{m,n}$ being the total number of Fourier modes, and l and l' represent the different interface labels for the Gateaux functional derivative *i.e.* Eqn.(45) and the derivative of Gateaux functional term. On expanding Eqn.(52) with respect to the co-ordinate representation of \mathbf{x}_l , the complete Hessian matrix is then written as a combination of sub-matrices

$$\mathcal{H} = \begin{bmatrix} \mathbf{H}_{j,k,l,l'}^{11} & \mathbf{H}_{j,k,l,l'}^{12} \\ \mathbf{H}_{j,k,l,l'}^{21} & \mathbf{H}_{j,k,l,l'}^{22} \end{bmatrix}, \quad (53)$$

where the sub-matrix quantities are written as

$$\mathbf{H}_{j,k,l,l'}^{11} = \frac{\partial}{\partial R_{l',k}} (\partial F_l / \partial R_{l,j}), \quad (54)$$

$$\mathbf{H}_{j,k,l,l'}^{12} = \frac{\partial}{\partial Z_{l',k}} (\partial F_l / \partial R_{l,j}), \quad (55)$$

$$\mathbf{H}_{j,k,l,l'}^{21} = \frac{\partial}{\partial R_{l',k}} (\partial F_l / \partial Z_{l,j}), \quad (56)$$

$$\mathbf{H}_{j,k,l,l'}^{22} = \frac{\partial}{\partial Z_{l',k}} (\partial F_l / \partial Z_{l,j}). \quad (57)$$

On Fourier decomposition, each sub-matrix quantities of Eqn.(53) can be written in block-tridiagonal structure as shown in Figure 2.

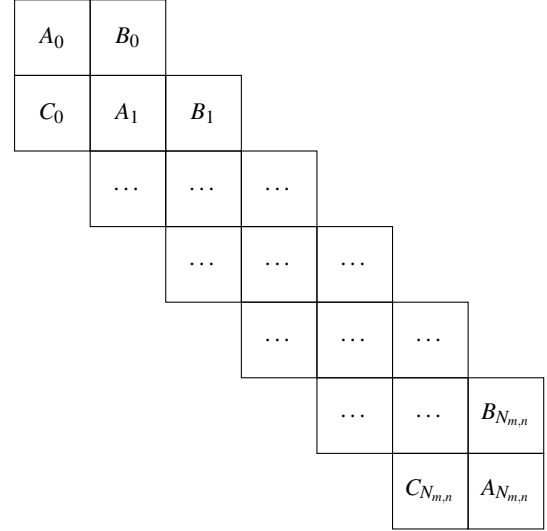


FIG. 2: Illustration of tri-diagonal arrangement of an $\mathbf{H}_{j,k,l,l'}^{11}$ matrix quantity defined in Eqn.(54) where $A_0 = \mathbf{H}_{j,k,l,l}^{11}$, $B_0 = \mathbf{H}_{j,k,l,l+1}^{11}$, $C_0 = \mathbf{H}_{j,k,l-1,l}^{11}$, $A_1 = \mathbf{H}_{j,k,l+1,l+1}^{11}$, $B_1 = \mathbf{H}_{j,k,l,l+2}^{11}$ and so on.

The Hessian \mathcal{H} is a matrix of size $N \times N$ where $N = (N_v - 1)N_{m,n}$ denotes the geometric degrees of freedom $N_{m,n} = n + 1 + m(2n + 1)$ is the total number of the Fourier modes.

As the Hessian matrix is symmetric, the quadratic form $\delta \mathbf{x}^T \cdot \mathcal{H} \cdot \delta \mathbf{x}$ can be decomposed into a set of real eigenvalues and an orthogonal basis of an eigenvectors, which is written as

$$\sum_{i=1}^N \mathbf{v}_i^T \cdot \mathcal{H} \cdot \mathbf{v}_i = \sum_{i=1}^N \lambda_i v_i^2, \quad (58)$$

where \mathbf{v}_i, λ_i are the eigenvectors and eigenvalues respectively. Since, \mathcal{H} is quadratic in displacement \mathbf{v}_i , our stability criterion are *necessary*, and *sufficient* for stability prediction. That is, the stability of MRxMHD equilibrium can be predicted from the sign of eigenvalue λ_i . If there exist an i such that $\lambda_i < 0$ then an equilibrium is said to be unstable and if all $\lambda_i > 0$ that is, positive then an equilibrium is said to be stable. By solving the eigenproblem for the Hessian, we obtain the direction of the steepest decay of F at the given location, which is determined by the eigenvector \mathbf{v}_i corresponding to the minimum eigenvalue $\lambda_{min} = \min(\lambda_i)$. Apparently, in doing so, an idea

of using SPEC-Hessian for an equilibrium sensitivity analysis and to reach the minimum energy or non-linear saturated states of unstable modes with a descent algorithm, emerges as an application. Intense investigation of this application is beyond the motive of this article and will be subject of a future publication.

We noticed that as the interfaces are perturbed to obtain Eqn.(52), the variation in magnetic field $\delta\mathbf{B}$ in SPEC can be determined using matrix perturbation theory by considering the Beltrami equation, $\nabla \times \mathbf{B} = \mu_l \mathbf{B}$ and $\mathbf{B} \cdot \mathbf{n} = 0$, and the enclosed fluxes as a constrained partial differential equation problem, where μ_l is a function of \mathbf{x}_l . This is consistent with solving the Eqns.(41), and also provides computational benefits. More insights of this procedure are supplied in Kumar *et al.*⁴¹ and Hudson *et al.*²⁴. In addition, the SPEC will consider the perturbed pressure, δp adiabatically with γ (usually 5/3) *i.e.* using the pressure-volume relation defined in Eqn.(8). Writing $p_l = \alpha_l/V_l^\gamma$ where $\alpha_l = \text{const.}$, the change in pressure p_l can be captured as change in corresponding volume V_l of relaxed plasma volumes Ω_l . Hence, the perturbed pressure is then computed as

$$\frac{\delta p_l}{p_l} = -\gamma \frac{\delta V_l}{V_l}, \quad (59)$$

where the $\delta V_l = \partial V_l / \partial R_l \delta R_l + \partial V_l / \partial Z_l \delta Z_l$. The corresponding expression of volume V_l in Eqn.(8) which is enclosed by the l^{th} and $l-1^{\text{th}}$ interface can be obtained by the integral

$$V_l = \int_{\Omega_l} d^3\tau = \frac{1}{3} \int_{\Omega_l} \nabla \cdot \mathbf{x}_l d^3\tau = \frac{1}{3} \int_{\delta\Omega_l} \mathbf{x}_l \cdot d\mathbf{S}, \quad (60)$$

$$= \frac{1}{3} \int_0^{2\pi} d\vartheta \int_0^{2\pi/N} d\zeta (\mathbf{x}_l \cdot \mathbf{e}_\vartheta \times \mathbf{e}_\zeta), \quad (61)$$

$$= \frac{1}{3} \int_0^{2\pi} d\vartheta \int_0^{2\pi/N} d\zeta R_l (Z_l R_{l,\vartheta} - R_l Z_{l,\vartheta}), \quad (62)$$

where we have used $\nabla \cdot \mathbf{x}_l = 3$, and have assumed that the domain is periodic in the angles. The required partial derivatives are computed as $\frac{\partial V_l}{\partial R_l}$ and $\frac{\partial V_l}{\partial Z_l}$ with their trigonometrical quantities. Details are shown in Appendix A.

IV. Numerical applications

In two magnetic configurations, that is, the tokamak and stellarator, the stability prediction and verification of SPEC-Hessian algorithm for MHD instabilities were studied numerically.

A. Verification in tokamak configuration

In this section, we undertake the verification study of our marginal stability prediction for two sub-classes of fixed boundary linear MHD instabilities in tokamaks *i.e.* the ideal internal kink and low shear ballooning modes. Incompressibility is assumed.

Ideal internal kink instability - Our marginal stability results of ideal internal kink instability have been verified with a well-known tokamak based incompressible ideal MHD stability code MISHKA-1⁵⁷. MISHKA-1 solves the linearised ideal MHD equations¹ with no flow for an eigenvalue $\tilde{\lambda} = \gamma + i\omega$, where γ is the linear growth rate of a mode with toroidal mode number n , and ω is the frequency of the mode. The linearised ideal MHD equations are found by treating all MHD variables in the form $X(t) = X_0 + \tilde{X}(t)$ for an equilibrium component X_0 and a small time-varying component $\tilde{X}(t) = \tilde{X} \exp(\tilde{\lambda}t)$, where the time-dependence comes from the assumption of the linear fluid perturbation $\xi(t) = \xi \exp(\tilde{\lambda}t)$, which also produces a linear magnetic field perturbation due to the frozen-in condition of ideal MHD. MISHKA-1 considers an ideal MHD equilibrium computed by the Grad-Shafranov equilibrium code HELENA⁵⁸.

Low shear ideal ballooning instability - We compare our low-shear stability results to global ideal MHD code, CAS3D^{59,60}. The CAS3D is designed to use the δW approach of ideal MHD energy principle⁵⁶ and treats the ideal MHD energy stability problem as variational form,

$$\lambda^{CAS3D} W_{kin}(\xi) - W_{pot}(\xi) = \text{minimum}, \quad (63)$$

in magnetic co-ordinates (s, θ, ϕ) to assess stability against global ideal MHD eigenmodes. Ideal instabilities of CAS3D are characterized by the sign of the lowest eigenvalue, λ_{min}^{CAS3D} in Eqn.(63), which is negative for an unstable equilibrium configuration. The sign of λ_{min}^{CAS3D} is completely decided by the definiteness properties of W_{pot} , with W_{kin} acting as kinetic normalization. The ideal MHD stability codes CAS3D and TERPSICHORE⁶¹ have been successfully verified for both the low shear stellarators and tokamaks. The CAS3D code is also used to verify the more recently developed CASTOR3D⁶² stability code. Of the late, CAS3D became an integral part of stellarator optimization package, ROSE (Rose Optimizes Stellarator Equilibria) code⁶³.

1. Ideal internal kink instability

In toroidal geometries, the internal kinks are mostly driven by the current density and pressure gradients, trying to twist magnetic flux surfaces into helical shapes, and further leads to topological reconnections (if *e.g.* resistivity is allowed). Specifically for monotonic q profiles, the internal kinks occurs when q_0 (value of safety factor at axis) falls below unity, when ohmic heating or current drive, drives the plasma current to peak at the magnetic axis in experimental operations.

Recently, an analysis of MRxMHD marginal stability prediction for the ideal internal kink instability has been conducted in a cylindrical tokamak, and shown good agreement with both the analytical theories and the M3D-C¹ calculation⁴¹. Because of an absence of poloidal coupling, toroidicity effects, and an assumption of pressureless plasma in that work, the prediction of ideal kink instability was less complicated. In this section, our stability has been analyzed with the details of the β -induced tokamak configura-

tion, where terms up to second order in inverse aspect ratio are examined, known as Bussac physics⁶⁴, for confirmation of SPEC Hessian predictions in toroidal geometry. For ideal internal kink instabilities in large aspect ratio tokamaks, Bussac *et al.*⁶⁴ derived an expression for marginal stability (*i.e.* when growth rate is zero) as

$$\beta_p = \frac{2}{B_\vartheta^2(\psi_s)} [\langle p(\psi) \rangle - p(\psi_s)], \quad (64)$$

where ψ_s and $B_\vartheta(\psi_s)$ are the corresponding poloidal flux and flux averaged magnetic poloidal field, evaluated at $q = 1$ rational surface respectively. Here, $\langle p(\psi) \rangle$ is the average pressure, defined as

$$\langle p(\psi) \rangle = \left(\int_0^{\psi_s} p(\psi) d\psi \right) / \psi_s. \quad (65)$$

The verification calculation is performed in an axisymmetric circular shaped large aspect ratio tokamak, where the parametric equations for the boundary harmonics in a cylindrical co-ordinate system (R, ϑ, Z) are determined with $R = R_0 + a \cos(\vartheta)$ and $Z = a \sin \vartheta$ with the major radius $R_0 = 10\text{m}$, and the minor radius $a = 1\text{m}$. The equilibrium parameters and pressure p and toroidal current j_ϕ have been considered as described in Mikhailovskii *et al.*⁶⁵ as

$$j_\phi = j_0(1 - \psi_p), \quad (66)$$

$$p = p_0(1 - \psi_p), \quad (67)$$

where ψ_p is the normalized poloidal flux. Note that close to magnetic axis $\psi_p \approx (r/a)^2$. Figure 3 shows an illustration of the equilibrium profiles with $q_0 < 1$ selected, so as be ideally unstable (for certain threshold of β_p).

In large-aspect ratio solutions, the safety factor q as the function of poloidal flux χ (let's assume) takes the form^{66,67}

$$q(\chi) = \frac{R_0 B_0 g(\chi)}{2\pi} \oint \frac{d\theta}{X^2 \mathbf{B} \cdot \nabla \theta}, \quad (68)$$

$$= q^{(0)}(r) + \varepsilon q^{(1)}(r, \theta) + \varepsilon^2 q^{(2)}(r, \theta) + \dots, \quad (69)$$

where the circular symmetry θ in lowest order is assumed with ε be inverse aspect ratio or the expansion parameter, $X = R_0 + r \cos \theta$, $g(\chi) = 1 + \varepsilon^2 g^{(2)}(r, \theta) + \dots$ where $\chi = \chi^0(r) + \varepsilon^2 \chi^{(1)}(r, \theta) + \dots$, and the integral is taken around the poloidal cross-section at constant χ . Then, in terms of zeroth-order $O(\varepsilon^0)$ the relation between the current density j_ϕ and safety factor q can be obtained as

$$q^{(0)}(r) = \frac{R_0}{B_0 r^2} \int_0^r r' j_\phi^{(0)}(r') dr', \quad (70)$$

where B_0 is the externally imposed toroidal magnetic field at the magnetic axis. Therefore, using the given pressure profile and q profile obtained with Eqn.(70), shown in see Figure 3, we first construct the ideal MHD based Variational Moments Equilibrium Code (VMEC) solution. The SPEC equilibrium input parameters are constructed by slicing the whole VMEC plasma volume into a certain N_v number of SPEC volumes. We have chosen the number of interfaces to be sufficiently large such that the marginal stability prediction does not show

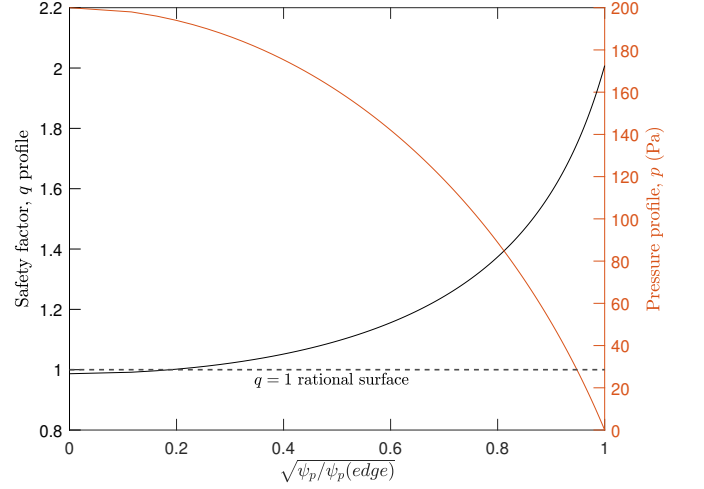


FIG. 3: Safety factor, q profile (in black) and pressure profile, p (in red) for $q_0 = 0.9866$ and $p_0 = 200$ Pa. Here, q_0 is defined as the value of safety factor on axis.

much changes. The SPEC's pressure profile as a function of poloidal flux in the l^{th} volume is computed from the VMEC solution as

$$p_l = \frac{1}{\psi_{p,l+1} - \psi_{p,l}} \int_{\psi_{p,l}}^{\psi_{p,l+1}} p(\psi_p) d\psi_p, \quad (71)$$

where $\psi_{p,l}$ and $\psi_{p,l+1}$ are the poloidal fluxes labelling the inner interface and outer interface of the l^{th} volume respectively. The continuous rotational transform profile from VMEC can be discretized over each interface as $\iota_l = \iota(\psi_{p,l})$, considering the field is integrable. The pressure profile supplied to SPEC is a stepped approximation to the VMEC pressure profile.

Note that because the pressure profile in SPEC is necessarily discontinuous, whereas the pressure profile used in the VMEC calculation is continuous and differentiable, there is necessarily a difference in the computed equilibria. This difference should reduce as the number of volumes increase, provided that the Fourier resolutions are sufficient enough to capture physics properties. To demonstrate and illustrate this point, we performed a self-convergence study of $(m, n) = (1, 1)$ eigenvalues from SPEC Hessian, as a function of N_v number of SPEC volumes, for the equilibrium when $q_0 = 0.95$ and $q_0 = 0.99$. The SPEC equilibrium configuration is computed by constraining the magnetic helicity, the poloidal and toroidal fluxes volume-wise, and the pressure in each Ω_l for the poloidal resolution, $m = \{0, 1, \dots, 12\}$ and the toroidal resolution $n = 0$. We have defined our maximum relative point-wise error as

$$E_\lambda^{1/1} = \frac{\max|\lambda - \lambda_{ref}|}{\max|\lambda_{ref}|}, \quad (72)$$

where the reference λ_{ref} are the values of λ_{SPEC} obtained with $N_v = 256$, for the β_p scan of corresponding q_0 , as shown in Figure 4. This error reliably decreases as the N_v is increased, at least up to the point where the relative error reaches close

to machine precision. Based on this error analysis, we can say that the $N_v = 180$, number of SPEC volumes is a reasonable approximation, for this ideal internal kink studies. This value is used in the remainder of this section.

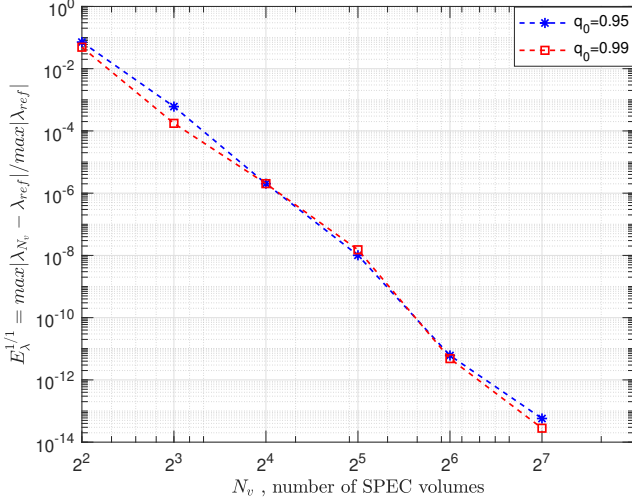


FIG. 4: Error $E_\lambda^{1/1}$ parameter defined in Eqn.(72) as a function of resolution parameter, N_v , for $m/n = 1/1$ eigenvalue, of stepped-pressure approximation. Here, the generalized SPEC stability matrix is computed for $m = \{0, 1, \dots, 12\}$ poloidal, and $n = 1$ toroidal mode spectrum.

Next, we proceed to compute and discuss our stability scans as a function of β_p for different q_0 . In Figure 5a the largest negative and smallest positive eigenvalues corresponding to $(m, n) = (1, 1)$ mode, obtained from the SPEC Hessian matrix are plotted as a function of β_p for different values of q_0 . Also shown in Figure 5b, the MISHKA-1 growth rates γ , normalized to Alfvén timescale, τ_A . The negative values of $\gamma\tau_A$ are obtained by extrapolation, for the required values of β_p . Figure 5c shows a comparison of the marginal stability locus, as predicted by SPEC Hessian and MISHKA-1 for the different values of q_0 obtained from Figure 5a and 5b. We found that as the number of volumes increases towards $N_v = 180$, the SPEC marginal stability points (coloured asterisk in Figure 5c) approaches ideal marginal stability predictions. Subsequently, in Figure 6, we compare the spatial dependence of radial eigenfunction of unstable $(m, n) = (1, 1)$ mode between SPEC and MISHKA-1 (with constant equilibrium number density profile, $\rho = 1$) calculation. The equilibrium with $q_0 = 0.99$ and $\beta_p = 0.297$ is considered. The normalized SPEC radial eigenfunction, $\xi_s^{m/n=1/1}$ is obtained by solving the Eqn.(54) for $\xi \cdot \mathbf{n}$. Hence, it appears to be a qualitative agreement between these two codes.

Moreover, the authors would like to remark that the comparison of the radial eigenfunction is well justified only for the values of β_p just across the marginal stability point, where the inertial effects can be negligible. Far away from the marginal stability threshold of β_p , there will be the significant dif-

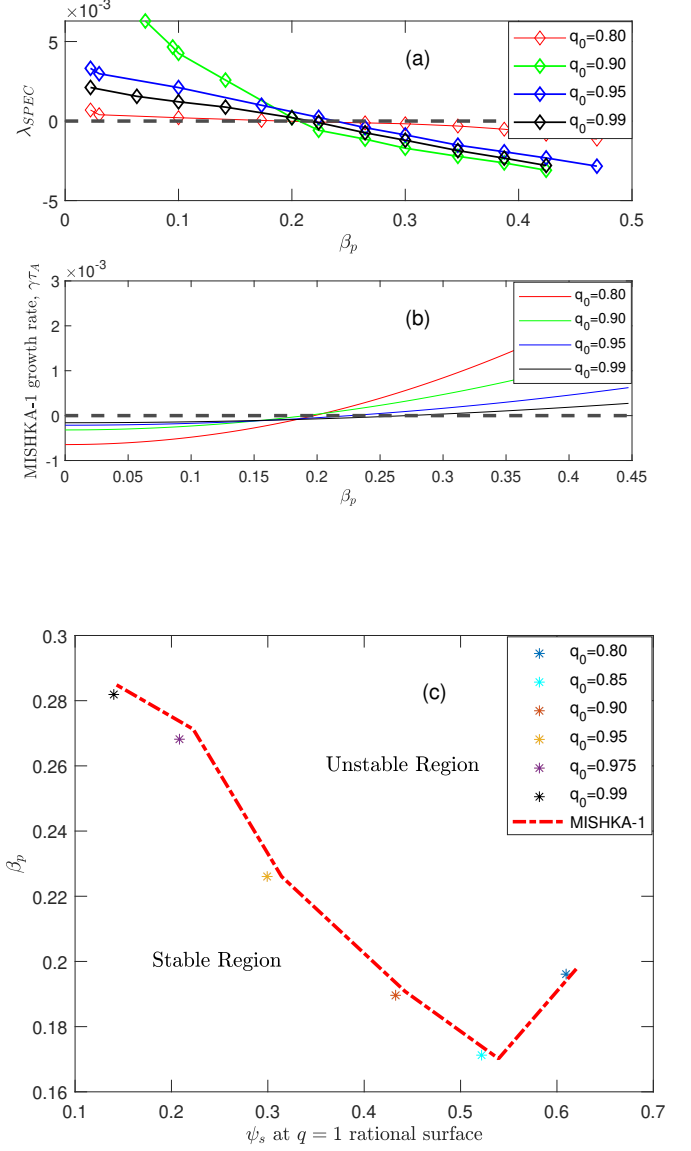


FIG. 5: For different scan of q_0 (a) λ_{SPEC} , the eigenvalues from Hessian matrix as a function of β_p , (b) the growth rate γ (solid lines) normalized to Alfvén timescale τ_A from MISHKA-1 ; (c) **Marginal stability locus** - the Bussac criterion β_p as a function of poloidal flux, ψ_s at the $q = 1$ rational surface for different choices of q_0 . The coloured asterisks are the β_p values obtained with SPEC and the solid curve (in red) is obtained with the ideal MHD code MISHKA-1.

ference in the radial eigenfunction, between our results and MISHKA-1. This is because of the lack of inertial effects in the SPEC calculation.

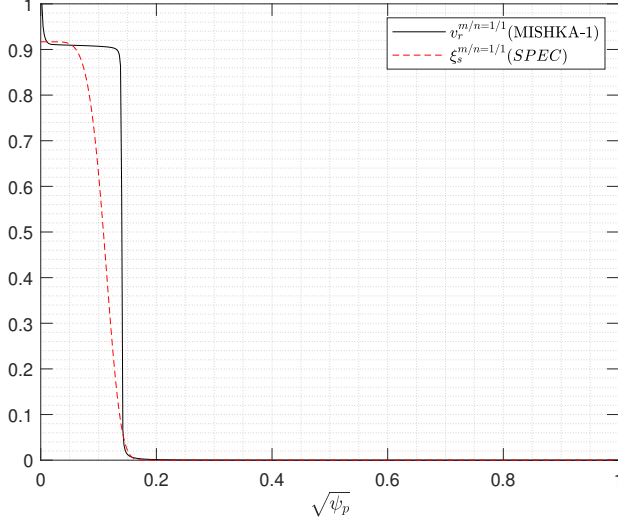


FIG. 6: Radial eigenfunctions $\xi_s^{m/n=1/1}$ and $v_r^{m/n=1/1}$, as a function of $\sqrt{\psi_p}$, for the unstable $m/n = 1/1$ ideal internal kink mode, when $q_0 = 0.99$.

2. Low-shear ballooning instability

Manickam, Pomphrey, and Todd⁶⁸ described the low shear ballooning instabilities commonly known as the "Infernal modes" are driven by a combination of shear and the pressure gradients. In tokamak plasmas these are unstable at values of the plasma beta that are below the threshold beta values of high- n ballooning theory, and when the value of the safety factor is approximately reduced to constant close to the plasma core. In this section, we demonstrate the validity of the finite- n SPEC Hessian approach to compute marginal stability of low shear ballooning modes with the global ideal MHD stability code CAS3D.

The choice of the verification configuration is as follows:

- A circular cross-sectional tokamak with an aspect ratio, $R_0/a (\equiv \varepsilon^{-1}) = 4$.
- The safety factor, q profile as function of poloidal flux of the form $q(\psi_p) = q_0 + q_1 \psi_p^\Gamma$ where $q_0 = 1.2$, $q_1 = 4.3$ and the q_{edge} can be obtained as $q_0 + q_1$. Here, we choose the value of Γ as 3 and 5.
- The pressure profile as a function of poloidal flux of the form $p(\psi_p) = p_0(1 - \psi_p)^2$.

Following Section IV A 1, we first choose to perform a VMEC calculation with the given pressure profile, q profile and aspect ratio such that the SPEC equilibrium input parameters are constructed by slicing up the VMEC plasma volume. The fixed boundary VMEC equilibrium calculation (here, the plasma boundary is given by $R_{0,0} = 4.0$, $Z_{0,0} = 0.0$, and $R_{1,0} = Z_{1,0} = 1.0$) is achieved with the Fourier harmonics $m \in \{0, 1, \dots, 30\}$, $n = 0$ and the radial flux surfaces, $N_s = 320$. Herein, it should be noted that the radial co-ordinates of both

SPEC and CAS3D is the normalized toroidal flux, so for our purpose we have transformed the above profiles in terms of toroidal flux.

The CAS3D stability calculations were performed with 320 flux intervals in a normalized toroidal flux grid for the perturbations Fourier harmonics $0 \leq m \leq M_{\text{max}}$ and $-2N_{\text{max}} \leq n \leq -N_{\text{max}}$ for specified value of $M_{\text{max}} = 30$ and $N_{\text{max}} = 3$. For both of the profile parameters $\Gamma = 3$ and $\Gamma = 5$, Figure 7a and 7b (top plots) plot the most unstable eigenvalues, $\lambda_{\text{min}}^{\text{CAS3D}}$, for the perturbation with globally dominant harmonic $(m, n) = (5, -4)$, as function of the scan over β_{axis} . This gives the approximated marginal stability values of $\beta_{\text{axis}} \approx 0.035$ for $\Gamma = 3$. And, on inspecting the CAS3D eigenvalues for the $\Gamma = 5$ case on a log-log plot, the stability limit that CAS3D finds is $\beta_{\text{axis}} \approx 0.0375$. The smallest two eigenvalues shown in Figure 7b would lead to a different slope in the eigenvalue versus β_{axis} regression. Furthermore, these two eigenvalues are most probably stable eigenvalues destabilized by the finite flux grid.

The SPEC equilibrium is defined by the toroidal flux enclosed by each interface, the pressure in each Ω_l , and the interface rotational transform. The input parameters are discretized over N_v number of volumes, where the enclosed toroidal flux in each region is chosen such that the total enclosed toroidal flux $\Delta\psi_l = 1$. In addition, since the pressure gradients are localized to ideal interfaces, the placement of the ideal interfaces also needs some specific attention. To avoid making the interface resonant with a mode (m, n) or its harmonics, we choose the rotational transform of each interface to be an irrational number, whose continued fraction expansion has an infinite sequence of 1's on its tail (also known as the Diophantine approximation⁶⁹). That is, for all integers n and m , there exists $r > 0$ and $k \geq 2$ such that a sufficiently irrational t must satisfy $|t - n/m| > r/m^k$. For ease of computation, a database of bounded-element irrational numbers⁷⁰ can also be constructed by iterating over continued fraction representations, or satisfying a property which is found in the Brjuno sets⁷¹.

To examine the stability properties of global MRxMHD stability, SPEC evaluates the Hessian matrix for the poloidal $m = \{0, 1, \dots, 30\}$ and the toroidal $n = \{-20, \dots, -1, 0, 1, \dots, 20\}$ (n spans as both positive and negative integers) mode spectrum. For both profile parameters $\Gamma = 3$ and $\Gamma = 5$, the stability scans were performed as a function of $\beta_{\text{axis}} (\equiv 2\mu_0 p_0 / B_0^2)$. The Figure 7c and 7d (middle plots) shows the most negative and smallest positive eigenvalues λ_{SPEC} , respectively for the perturbation with most dominant harmonic $(m, n) = (5, -4)$, which means that it fulfills the resonance condition, $mt + n = 0$. For fixed N_v , as β_{axis} increases, the plasma destabilizes after it crosses the threshold value, which leads to the violation of ballooning stability. Later on, it is observed that as N_v increases (depicted in Figure 7c and 7d), the marginal stability thresholds predicted by SPEC gradually converge towards the IMHD stability threshold (predicted by CAS3D). Specifically, in Figure 7c at $N_v = 250$, the stability threshold/limit is quite similar to the Figure 7a of CAS3D, that is, $\beta_{\text{axis}} \approx 0.035$. This is expected because, the MRxMHD energy principle is based on the constraints which are the subset of the IMHD

topological invariants, hence the space of allowed variations in MRxMHD is larger than that allowed by ideal MHD but includes it as a subspace. As such, the numerical properties of isotropic MRxMHD model will also be a bit different from IMHD, and this model can converge towards the IMHD equilibrium and its stability theories. A formal theoretical proof of convergence may in general be difficult at this stage, but will be a subject of future research. In other works, Dennis *et al.*⁷² and Hudson *et al.*³² have studied the convergence of stepped pressure equilibria (with SPEC) towards the VMEC equilibria. Now in the other case $\Gamma = 5$, in Figure 7c, at $N_v = 260$ it can be observed that, it is not possible to easily define an exact threshold, as the λ_{SPEC} remains negative. However, one may approximate the threshold as $\beta_{axis} \approx 0.0375$ based on the eigenvalues' trend. That is, below the approximated value of marginal stability limit $\beta_{axis} \approx 0.0375$, the values of λ_{SPEC} (in Figure 7d) remain stagnant and nearly unchanged, which can be interpreted as numerical artifacts. This is well consistent with the behaviour of eigenvalues determined by CAS3D Figure 7b. Nevertheless, even for $\Gamma = 5$, the SPEC stability limit tends to progressively converge towards the estimated IMHD stability threshold as N_v increases from 160,... to 260.

In particular, the driving term associated with the instability arises from the unfavourable curvature (curvature data not shown) and the local shear that are encapsulated through the modified Pfirsch-Schlüter current defined on interfaces. Figures 8a - 8d show the dominant mode structure for the unstable values of β_{axis} via the Fourier modes' amplitudes versus radial coordinate (the normalized toroidal flux), for values of $\Gamma = 3$ and 5. For the case when $\Gamma = 3$ and $N_v = 250$, the SPEC stability limit and eigenmode structures depicted in Figures 7c and 8a respectively, are found to be relatively comparable to CAS3D (see Figure 8c). In contrast, when $\Gamma = 5$ and $N_v = 260$, the approximated SPEC stability limit depicted in Figure 7d is found to be quite satisfactory when compared to CAS3D, however the eigenmode structures (shown in Figure 8b) persists a small discrepancy to the CAS3D Figure 8d. That is, the maxima of the dominant (5, -4) harmonic in Figures 8b and 8d do not coincide but have very similar sidebands. Even so, the mode structures are clearly observed in the regions localized to resonant rational surfaces (that is, near $\iota = 0.8$ or $q = 1.25$) with higher pressure gradient and low magnetic shear. And that is why the low-shear ballooning modes (infernal modes) are characterized differently in IMHD than the pure ballooning modes. Which means, the ballooning modes in tokamaks couple with many Fourier components, and does not strongly single out one rational surface. The low-shear ballooning or the infernal modes, in contrasts, are sensitive to a particular rational surface (here, $q = 1.25$) and strongly singles it out by a burst of instability when this surface is close to or near the plasma core. This is also evident from the unstable eigenfunction plots in Figures 8a to 8d.

Now, in order to quantify whether these instabilities are infernal modes or not, we use the WKB theory of ballooning modes to describe it. In literature of ballooning instability, the standard Wentzel-Kramers-Brillouin (WKB) ideal ballooning theory is shown to break when the shear is reduced or lowered⁷³, for moderately low toroidal mode number n . The

numerical solution of this ideal ballooning WKB formalism can be obtained by COBRAVMEC code⁷⁴. This code numerically solves the ideal MHD ballooning equation in magnetic co-ordinates (s, θ, ζ) to assess the stability against ideal ballooning modes. The ballooning instability of COBRAVMEC is characterized by the positive growth rate normalized to Alfvén timescale, and has been calculated on the poloidal and toroidal grid of each flux surface of VMEC¹⁴ equilibrium.

Therefore, as with SPEC and CAS3D, with COBRAVMEC we seek for the threshold marginal stability value of β_{axis} , where the plasma destabilizes and violates ballooning stability. For various scan over β_{axis} , the Figure 9a and 9b shows the ballooning growth rates as a function of ψ_w (normalized flux) from COBRAVMEC. For our profile parameter $\Gamma = 3$ and $\Gamma = 5$, COBRAVMEC predicts the marginal stability threshold value as $\beta_{axis} = 0.038718$ and $\beta_{axis} = 0.0443$ respectively, to three significant figures. Now it can be seen, at $\beta_{axis} = 0.041315$ (for $\Gamma = 5$), COBRAVMEC predicts that the plasma is stable to ballooning modes, but the both CAS3D and SPEC shows that the plasma is unstable. This can be characterized by the plots presented in Figures 8b-8d for the unstable dominant mode structure obtained with both CAS3D and SPEC calculations. And that is where the pure WKB ballooning theory shows its fragility to analyze the low shear plasma at low plasma beta. Also, for the case of $\Gamma = 3$ at $\beta_{axis} = 0.038718$, according to ballooning theory of COBRAVMEC, the mode is stable, but there exists an unstable mode at this beta value, which has also been shown by SPEC and CAS3D. Now, note that when we change the Γ from 3 to 5, the plasma shear near the core decreases (which can be seen from the q profile or rotational transform profile). And, as a result, in tokamak plasmas, it is important to maintain the magnetic shear near the core or, throughout the mid of the plasma, to avoid this kind of MHD instabilities. Apart from this, increasing to higher values of plasma beta causes these infernal modes to change to pure ballooning mode instability, allowing the principles of the ideal WKB ballooning theory to be implemented⁶⁸.

Altogether Figures 7, 8 and 9 summarize the SPEC and CAS3D stability predictions and their behaviour of low-order harmonics of infernal modes in the resonant subset of the mode spectrum. As we identified, once the infernal instability is reached at low-shear plasma regime for low-beta, it may be irrelevant to increase beta any further, and the oscillations at higher beta may be out of academic interest.

B. Verification in geometrically simple stellarator configuration

In many aspects, the MHD and stability properties in stellarators are quite different from those in axisymmetric tokamaks. The external magnetic fields in stellarators can provide the requisite rotational transform for confinement without the need of a net plasma current, hence, the MHD instabilities driven by such a current are absent. But, since stellarators are generally low-shear devices, the low- n MHD instabilities potentially produce magnetic fluctuations at finite plasma beta.

In fact at certain plasma beta, the pressure-driven Pfirsch-Schlüter currents lead to the Shafranov shift and incite MHD instability. Therefore, in this section we focus on the investigation of a beta scan of a stellarator equilibrium, and determine the stability β -limit.

Our stellarator configuration and its equilibrium parameters are defined in the following way. The Fourier coefficients $R_{m,n}$ and $Z_{m,n}$ that approximate the shape of plasma boundary in SPEC are given in TABLE 1. The three characteristic plasma cross-sections of our plasma boundary, for $\langle\beta\rangle = 0.02$, are shown in Figure 10a. The figure 10b shows the three-dimensional plot of the plasma boundary illustrating the 3-D nature of the configuration.

Due to the discrete symmetry of stellarators (with a finite number of identical field periods), the concept of decoupled mode families applies in stellarator MHD stability calculations. This is the analogue of the complete decoupling in the toroidal direction for the axisymmetric tokamaks. As a matter of fact, in axisymmetric tokamaks the toroidal mode number can be considered a good quantum number, since the equilibrium fields include only $n = 0$ and provide no coupling between instabilities having different n values. For stellarators with N_p field period, the Fourier harmonics with toroidal mode number n are coupled to $n + kN_p$, where k is an arbitrary integer. Standardly, there are $N_p/2 + 1$ families of modes for even N_p and $(N_p - 1)/2 + 1$ families for odd N_p . For example, for $N_p = 2$ and 3, there exists two mode families $N = 0$ and 1. In our five-periodic stellarator configuration (for $N_p = 5$) there are three such mode families⁶⁰ with the generating toroidal Fourier numbers $N = 0, 1, 2$. Figure 11 shows the relationship between these mode families and rational rotational transforms of our five-periodic case, which also applies to the Wendelstein 7-X (W7-X) configuration to some extent. One must be careful that here n represents the toroidal mode number, while N denotes the mode family index.

The Figure 12a compares the marginal stability threshold between the SPEC and CAS3D, as a function of $\langle\beta\rangle$. Appendix B comprises a thorough description of SPEC and VMEC equilibrium construction to obtain required rotational transforms at varied volume-averaged plasma beta. In both SPEC and CAS3D runs, the unstable perturbation is dominated by $(m, n) = (10, -11)$ if the $N = 1$ mode family is considered. Furthermore, Figure 12b shows the radial behaviour of dominant Fourier coefficients of the normal component of the displacement, $\xi_5^{m,n}$ (from SPEC) at $\langle\beta\rangle = 0.01$ which is unstable. In the CAS3D runs, the normal displacement (shown in Figure 12c) is the component of the ideal MHD displacement vector in the direction of the outer magnetic surface normal, which is here approximated using 153 total number of Fourier harmonics. Their radial dependence is determined by solving the linearized ideal MHD equation in a weak form, Eqn.(63).

It is evident from Figure 12b and 12c that the mode is radially localised and has few competing amplitude Fourier harmonics, which is somewhat analogous to the characteristics of low- n ballooning modes in tokamaks. As obvious, the radial structure of the global, unstable mode also demonstrates that its maximum amplitude is located near the respective res-

TABLE I: Fourier coefficients of representing an outer magnetic surface (plasma boundary) in SPEC of our five field period ($N_p = 5$) stellarator variant.

n	m	$R_{bc,m,n}$	$Z_{bs,m,n}$
0	0	5.500000×10^0	0.000000×10^0
1	0	2.402972×10^{-1}	-1.160280×10^{-1}
2	0	4.139300×10^{-3}	-3.081540×10^{-3}
3	0	5.780720×10^{-4}	-5.780720×10^{-4}
-3	1	-8.008660×10^{-4}	-8.008660×10^{-4}
-2	1	-1.513380×10^{-2}	-1.513380×10^{-2}
-1	1	-2.696804×10^{-1}	-2.696804×10^{-1}
0	1	5.065566×10^{-1}	-5.573040×10^{-1}
1	1	3.124000×10^{-4}	-3.124000×10^{-4}
2	1	6.453700×10^{-4}	-6.441820×10^{-4}
3	1	1.946472×10^{-5}	-1.946472×10^{-5}
-4	2	-2.381500×10^{-4}	-2.381500×10^{-4}
-3	2	-2.106786×10^{-3}	-1.505504×10^{-3}
-2	2	2.200000×10^{-2}	2.200000×10^{-2}
-1	2	3.694460×10^{-2}	-4.564120×10^{-2}
0	2	2.388980×10^{-2}	-2.330460×10^{-2}
1	2	1.864126×10^{-3}	-1.864126×10^{-3}
-4	3	1.394998×10^{-3}	1.394998×10^{-3}
-3	3	-2.031524×10^{-3}	-2.031524×10^{-3}
-2	3	2.279420×10^{-3}	-2.279420×10^{-3}
-1	3	3.679940×10^{-3}	3.679940×10^{-3}
0	3	1.035166×10^{-3}	-1.035166×10^{-3}
-3	4	-1.185624×10^{-3}	-1.185624×10^{-3}
-2	4	-2.889040×10^{-3}	2.889040×10^{-3}

onant rotational transform, $\iota = 11/10$ when $\langle\beta\rangle = 0.01$ (see the $\iota = 11/10$ rational surface in Figures 13a and 13b of Appendix B).

On taken together Figures 12a, 12b and 12c, we conclude that the SPEC prediction in this geometrically simple stellarator configuration implies MHD instabilities with similar characteristics to the CAS3D runs and shows a qualitative agreement.

V. Comments and future work

The Stepped Pressure Equilibrium Code (SPEC) has been extended to predict linear MHD instabilities with Multi-Region relaxed MHD energy principle. Based on the variational formulation of MRxMHD energy functional, the Hessian algorithm (generalized stability matrix) that contains the second variation of the MRxMHD energy functional is formulated to analyze MRxMHD stability in toroidal geometry. Our formalism is general as it did not use the assumption of axisymmetry. Negative eigenvalues of the Hessian matrix represent the instability of an equilibrium.

In this work, the authors performed the first numerical verification of SPEC for the pressure-driven ideal MHD like instabilities of MRxMHD in both tokamak and stellarator geometries. For axisymmetric plasma, we have considered a circular tokamak equilibria, where the SPEC/MRxMHD-Stability

results, such as, the marginal stability limits and eigenmode structures are compared with MISHKA-1 and CAS3D. For non-axisymmetric plasma, we have considered a five field period stellarator equilibrium, where the stability predictions and dominant mode structure are compared with CAS3D. In doing so, we have demonstrated the efficacy of MRxMHD-Stability to predict pressure-driven ideal MHD instabilities, as well as the numerical feasibility of solving challenging stepped-pressure MHD stability analyses.

Moreover, most of the physics codes in the stellarator community first determine a plasma equilibrium, *e.g.* using VMEC, and then call a separate MHD stability code such as CAS3D. In the more recent complementary work of Aleynikova *et al.*⁷⁵, SPEC was employed to evaluate the MRxMHD equilibrium and stability simultaneously in simplified Wendelstein 7-X stellarator geometry. That work has been devoted to the understanding the nature of the crashes in Electron Cyclotron Current Drive controlled scenarios in W7-X plasmas.

The development of stability studies performed in this work using SPEC, enables several avenues of future work. As an example, the study of the direct comparison of MRxMHD stability with experimental data of well-known high n ballooning instabilities, and utilization in stellarator optimizations loops are included in our research plan. We also plan to employ our approach to investigate MHD modes such as interchange modes, and the stability convergence versus N_v , as a future effort for more complicated analysis in 3D plasma geometries. While we aim to undertake more 3D MHD or high- n stability computations in near the future, various code development work (as pointed out in Hudson *et al.*³²) must be completed in parallel, in order for SPEC to be more efficient and robust in 3D.

In principle, the variational approach within the MRxMHD formulation is rather different from the conventional ideal MHD variational approach, as the magnetic fields are allowed to tear and form magnetic islands and stochastic fields. This is enabled by the Taylor relaxation within each volumes, which allows reconnection at rational surfaces like resistive MHD. As such it would be interesting to study linear resistive MHD instability in addition to the ideal MHD stability theory. Stability of such equilibria can also be accessed using the same SPEC Hessian calculation. In particular, the recent investigation of SPEC Hessian calculation on the prediction of tearing instability in pressureless slab^{30,31} and cylindrical plasma⁴¹ reports an excellent agreement with tearing criterion Δ' . To extend the work to tearing modes for axisymmetric tokamaks, we would require an extensive well-designed study of a new resistive volume layer theory of MRxMHD with inertial effects, and comparison with Glasser, Greene, Johnson compressible model⁶⁷ or any other resistive MHD codes. That is, using an incompressible model for tearing modes in toroidal plasma appears to be an evident contradiction. The tearing modes are quite sensitive to pressure even at very low plasma β values⁷⁶. As pressure increases, the transition from an incompressible to a compressible plasma occurs at β levels that are required to achieve high β plasma confinements. Thus, whether the compressible plasma should be considered in

MRxMHD volume layer theory is still an outstanding question that has yet to be answered.

In tokamak geometry the toroidal mode number n is a good quantum number. Singular points occur where $q = m/n$, hence they are well-separated in flux. For non-axisymmetric systems, both m and n are coupled, and the singular surfaces are densely packed (also known as quantum chaos) in plasma, limited only by truncation of the basis functions. Therefore, the full treatment of resistive modes in MRxMHD and SPEC is a challenging problem, requiring further theoretical and computational development.

Along with these future developments, recently the fixed boundary SPEC has been extended to calculate free-boundary MRxMHD equilibria³². Hence, we believe that it is also possible to extend the capabilities of the Hessian algorithm to the free-boundary version of SPEC, such as to encapsulate the free-boundary MHD instabilities. (See Henneberg *et al.*⁷⁷ for the more detailed exposition of how to calculate the matrix quantities for free-boundary instability, defined in terms of a primitive set of equilibrium quantities used by SPEC.)

Acknowledgments

The authors would like to acknowledge Samuel Lazerson, Per Helander, Wilfred A. Cooper, Adelle Wright, Caoxiang Zhu, and the collaborators of Simons Collaboration on Hidden Symmetries and Fusion Energy (HSFE) for their valuable insights and fruitful suggestions. Matthew Hole gratefully acknowledges the support of G. A. Huysmans from CEA Cadarache in the provision of HELENA and MISHKA codes.

This research is based upon work supported by the Australian Research Council (ARC) project No. DP170102606 and a grant from the Simons Foundation/SFARI No. 560651/AB. Joaquim Loizu work has been carried out in part within the framework of the EUROfusion consortium and has received funding from the Euratom research and training programme 2014-2018 and 2019-2020 under grant agreement No. 633053. The views and opinions expressed herein do not necessarily reflect those of the European Commission. This research is undertaken with the assistance of resources and services from the National Computational Infrastructure GADI (200 nodes each contains two 24-core Intel Xeon Scalable ‘Cascade Lake’ processors), which is supported by the Australian Federal Government in the framework of ANU Merit Allocation Scheme.

A. Calculation of perturbed volume quantities in SPEC

In this Appendix, we present the expression of perturbed volume in SPEC. The volume in SPEC enclosed by adjacent interfaces is given as

$$V_l = \frac{1}{3} \int_0^{2\pi} d\vartheta \int_0^{2\pi/N} d\zeta R_l (Z_l R_{l,\vartheta} - R_l Z_{l,\vartheta}). \quad (\text{A1})$$

On expanding the above equation in summation of the Fourier harmonics, we have

$$V_l = \frac{1}{3} \sum_i \sum_j \sum_k R_{l,i} (Z_{l,j} R_{l,k} - R_{l,j} Z_{l,k}) (+m_k) \quad (\text{A2})$$

$$\times \oint \oint \cos \alpha_i \cos \alpha_j \cos \alpha_k d\vartheta d\zeta,$$

where i^{th} , j^{th} and k^{th} are the Fourier harmonics of R_l, Z_l .

Then, the partial derivatives $\frac{\partial V_l}{\partial R_{l,i}}$ and $\frac{\partial V_l}{\partial Z_{l,i}}$ are obtained as

$$3 \frac{\partial V_l}{\partial R_{l,i}} = (Z_{l,j} R_{l,k} m_k - R_{l,j} Z_{l,k} m_k - R_{l,j} Z_{l,k} m_k) \quad (\text{A3})$$

$$\times \oint \oint \cos \alpha_i \cos \alpha_j \cos \alpha_k$$

$$+ (-Z_{l,j} R_{l,k} m_k + R_{l,j} Z_{l,k} m_k + R_{l,j} Z_{l,k} m_k)$$

$$\times \oint \oint \cos \alpha_i \sin \alpha_j \sin \alpha_k,$$

and

$$3 \frac{\partial V_l}{\partial Z_{l,i}} = (-R_{l,k} R_{l,j} m_i) \oint \oint \cos \alpha_i \cos \alpha_j \cos \alpha_k \quad (\text{A4})$$

$$+ (-R_{l,k} R_{l,j} m_k) \oint \oint \cos \alpha_i \sin \alpha_j \sin \alpha_k.$$

B. Stellarator equilibria with VMEC and SPEC

The CAS3D stability code is interfaced to the ideal MHD equilibrium code VMEC. Input data for the VMEC code are the R and Z Fourier coefficients of the plasma boundary (R, Z, ϕ) cylindrical coordinates. Note that the VMEC and SPEC boundary Fourier coefficients differ only in sign (stemming from different notations used and handedness), which is described as $R_{bc,m,n}^{SPEC} = +R_{bc,m,-n}^{VMEC}$ and $Z_{bs,m,n}^{SPEC} = -Z_{bs,m,-n}^{VMEC}$. Other subtleties are discussed in Hudson *et al.*²⁴. The rotational transform profiles of equilibria with vanishing net toroidal current are shown in Figure 13a and 13b respectively. The pressure profile was used in form of a power series: $P(s) = P_0(1 - 1.31553s + 0.14126s^2 + 0.17427s^3)$, where s is the normalized toroidal flux and P_0 a scaling factor in units of pressure. The SPEC equilibrium profiles are discretized over 16 volumes. The Poincaré cross-sections at toroidal angle $\phi = 0^\circ$ obtained with SPEC and VMEC are shown in 14a and 14b.

- ¹J. P. Freidberg, "Ideal magnetohydrodynamic theory of magnetic fusion systems," *Rev. Mod. Phys.* **54**, 801–902 (1982).
- ²W. Tang, R. Dewar, and J. Manickam, "Influence of diamagnetic drifts on critical beta in tokamaks," *Nuclear Fusion* **22**, 1079–1081 (1982).
- ³The pressure is understood to be in units of $\mu_0 \times [J/m^3]$ where $\mu_0 = 4\pi \times 10^{-7} [H/m]$, μ_0 is the vacuum permeability.
- ⁴T. Amari, C. Boulbe, and T. Z. Boulmezaoud, "Computing Beltrami Fields," *SIAM Journal on Scientific Computing* **31**, pp. 3217–3254 (2009).
- ⁵G. Alkauskas, "Beltrami vector fields with an icosahedral symmetry," *Journal of Geometry and Physics* **153**, 103655 (2020).
- ⁶I. Nunes and *et al.*, "Plasma confinement at JET," *Plasma Physics and Controlled Fusion* **58**, 014034 (2015).

- ⁷S. A. Lazerson and I. T. Chapman, "STELLOPT modeling of the 3d diagnostic response in ITER," *Plasma Physics and Controlled Fusion* **55**, 084004 (2013).
- ⁸J.-K. Park, S. M. Yang, N. C. Logan, Q. Hu, C. Zhu, M. C. Zarnstorff, R. Nazikian, C. Paz-Soldan, Y. M. Jeon, and W. H. Ko, "Quasisymmetric optimization of nonaxisymmetry in tokamaks," *Phys. Rev. Lett.* **126**, 125001 (2021).
- ⁹J. W. Burby, N. Kallinikos, and R. S. MacKay, "Generalized grad-shafranov equation for non-axisymmetric mhd equilibria," *Physics of Plasmas* **27**, 102504 (2020), <https://doi.org/10.1063/5.0015420>.
- ¹⁰A. H. Boozer, "Plasma equilibrium with rational magnetic surfaces," *The Physics of Fluids* **24**, 1999–2003 (1981), <https://aip.scitation.org/doi/pdf/10.1063/1.863297>.
- ¹¹H. Grad, "Toroidal containment of a plasma," *The Physics of Fluids* **10**, 137–154 (1967), <https://aip.scitation.org/doi/pdf/10.1063/1.1761965>.
- ¹²A. Bhattacharjee, T. Hayashi, C. C. Hegna, N. Nakajima, and T. Sato, "Theory of pressure-induced islands and self-healing in three-dimensional toroidal magnetohydrodynamic equilibria," *Physics of Plasmas* **2**, 883–888 (1995), <https://doi.org/10.1063/1.871369>.
- ¹³S. R. Hudson and B. F. Kraus, "Three-dimensional magnetohydrodynamic equilibria with continuous magnetic fields," *Journal of Plasma Physics* **83**, 715830403 (2017).
- ¹⁴S. Hirshman, W. van Rij, and P. Merkel, "Three-dimensional free boundary calculations using a spectral green's function method," *Computer Physics Communications* **43**, 143–155 (1986).
- ¹⁵J.-k. Park, A. H. Boozer, and A. H. Glasser, "Computation of three-dimensional tokamak and spherical torus equilibria," *Physics of Plasmas* **14**, 052110 (2007), <https://doi.org/10.1063/1.2732170>.
- ¹⁶A. Reiman and H. Greenside, "Calculation of three-dimensional mhd equilibria with islands and stochastic regions," *Computer Physics Communications* **43**, 157–167 (1986).
- ¹⁷S. P. Hirshman, R. Sanchez, and C. R. Cook, "Siesta: A scalable iterative equilibrium solver for toroidal applications," *Physics of Plasmas* **18**, 062504 (2011), <https://doi.org/10.1063/1.3597155>.
- ¹⁸Y. Suzuki, N. Nakajima, K. Watanabe, Y. Nakamura, and T. Hayashi, "Development and application of HINT2 to helical system plasmas," *Nuclear Fusion* **46**, L19–L24 (2006).
- ¹⁹M. Rampp, R. Preuss, R. Fischer, and t. Team, "Gpec, a real-time capable tokamak equilibrium code," *arXiv:1511.04203* (2015), 10.13182/FST15-154.
- ²⁰J. B. Taylor, "Relaxation and magnetic reconnection in plasmas," *Rev. Mod. Phys.* **58**, 741–763 (1986).
- ²¹O. P. Bruno and P. Laurence, "Existence of three-dimensional toroidal mhd equilibria with nonconstant pressure," *Communications on Pure and Applied Mathematics* **49**, 717–764 (1996).
- ²²R. L. Dewar, M. J. Hole, and S. R. Hudson, "Piecewise-beltrami mhd equilibria," (APS April meeting, 2006) <http://meetings.aps.org/link/BAPS.2006.APR.P16.2>.
- ²³R. Dewar, Z. Yoshida, A. Bhattacharjee, and S. Hudson, "Variational formulation of relaxed and multi-region relaxed magnetohydrodynamics," *Journal of Plasma Physics* **81**, 515810604 (2015).
- ²⁴S. R. Hudson, R. L. Dewar, G. Dennis, M. J. Hole, M. McGann, G. von Nessi, and S. Lazerson, "Computation of multi-region relaxed magnetohydrodynamic equilibria," *Physics of Plasmas* **19**, 112502 (2012), <https://doi.org/10.1063/1.4765691>.
- ²⁵G. R. Dennis, S. R. Hudson, D. Terranova, P. Franz, R. L. Dewar, and M. J. Hole, "Minimally constrained model of self-organized helical states in reversed-field pinches," *Phys. Rev. Lett.* **111**, 055003 (2013).
- ²⁶J. Loizu, S. R. Hudson, P. Helander, S. A. Lazerson, and A. Bhattacharjee, "Pressure-driven amplification and penetration of resonant magnetic perturbations," *Physics of Plasmas* **23**, 055703 (2016), <https://doi.org/10.1063/1.4944818>.
- ²⁷J. Loizu, S. R. Hudson, A. Bhattacharjee, S. Lazerson, and P. Helander, "Existence of three-dimensional ideal-magnetohydrodynamic equilibria with current sheets," *Physics of Plasmas* **22**, 090704 (2015), <https://doi.org/10.1063/1.4931094>.
- ²⁸J. Loizu, S. R. Hudson, C. Nührenberg, J. Geiger, and P. Helander, "Equilibrium beta-limits in classical stellarators," *Journal of Plasma Physics* **83**, 715830601 (2017).
- ²⁹A. Baillod, J. Loizu, Z. S. Qu, A. Kumar, and J. Graves, "Computation of

- mrxmhd equilibria with prescribed toroidal current profile,” (2021), (accepted for publication in Journal of Plasma Physics).
- ³⁰J. Loizu and S. R. Hudson, “Multi-region relaxed magnetohydrodynamic stability of a current sheet,” *Physics of Plasmas* **26**, 030702 (2019), <https://doi.org/10.1063/1.5091765>.
- ³¹J. Loizu, Y.-M. Huang, S. R. Hudson, A. Baillo, A. Kumar, and Z. S. Qu, “Direct prediction of nonlinear tearing mode saturation using a variational principle,” *Physics of Plasmas* **27**, 070701 (2020), <https://doi.org/10.1063/5.0009110>.
- ³²S. R. Hudson, J. Loizu, C. Zhu, Z. S. Qu, C. Nührenberg, S. Lazerson, C. B. Smiet, and M. J. Hole, “Free-boundary MRxMHD equilibrium calculations using the stepped-pressure equilibrium code,” *Plasma Physics and Controlled Fusion* **62**, 084002 (2020).
- ³³G. R. Dennis, S. R. Hudson, R. L. Dewar, and M. J. Hole, “Multi-region relaxed magnetohydrodynamics with anisotropy and flow,” *Physics of Plasmas* **21**, 072512 (2014), <https://doi.org/10.1063/1.4890847>.
- ³⁴M. Lingam, H. M. Abdelhamid, and S. R. Hudson, “Multi-region relaxed hall magnetohydrodynamics with flow,” *Physics of Plasmas* **23**, 082103 (2016), <https://doi.org/10.1063/1.4960128>.
- ³⁵R. L. Dewar, L. H. Tuen, and M. J. Hole, “The spectrum of multi-region-relaxed magnetohydrodynamic modes in topologically toroidal geometry,” *Plasma Physics and Controlled Fusion* **59**, 044009 (2017).
- ³⁶R. L. Dewar, J. W. Burby, Z. S. Qu, N. Sato, and M. J. Hole, “Time-dependent relaxed magnetohydrodynamics: Inclusion of cross helicity constraint using phase-space action,” *Physics of Plasmas* **27**, 062504 (2020), <https://doi.org/10.1063/5.0005740>.
- ³⁷R. L. Dewar, J. W. Burby, Z. S. Qu, N. Sato, and M. J. Hole, “Time-dependent relaxed magnetohydrodynamics: Inclusion of cross helicity constraint using phase-space action,” *Physics of Plasmas* **27**, 062504 (2020), <https://doi.org/10.1063/5.0005740>.
- ³⁸M. D. Kruskal and R. M. Kulsrud, “Equilibrium of a magnetically confined plasma in a toroid,” *The Physics of Fluids* **1**, 265–274 (1958).
- ³⁹M. D. Kruskal and C. R. Oberman, “On the stability of plasma in static equilibrium,” *The Physics of Fluids* **1**, 275–280 (1958), <https://aip.scitation.org/doi/pdf/10.1063/1.1705885>.
- ⁴⁰J. M. Greene, “A new form of the magnetohydrodynamic potential energy,” *Physics of Plasmas* **3**, 8–9 (1996), <https://doi.org/10.1063/1.871828>.
- ⁴¹A. Kumar, Z. Qu, M. J. Hole, A. M. Wright, J. Loizu, S. R. Hudson, A. Baillo, R. L. Dewar, and N. M. Ferraro, “Computation of linear MHD instabilities with the multi-region relaxed MHD energy principle,” *Plasma Physics and Controlled Fusion* **63**, 045006 (2021).
- ⁴²A. Almagri, D. Anderson, F. Anderson, P. Probert, J. Shohet, and J. Talmadge, “A helically symmetric stellarator (hsx),” *IEEE Transactions on Plasma Science* **27**, 114–115 (1999).
- ⁴³T. Klinger, T. Andreeva, and W. Team, “Overview of first wendelstein 7-x high-performance operation,” *Nuclear Fusion* **59**, 112004 (2019).
- ⁴⁴A. H. Glasser, C. R. Sovinec, R. A. Nebel, T. A. Gianakon, S. J. Plimpton, M. S. Chu, D. D. Schnack, and the NIMROD Team, “The NIMROD code: a new approach to numerical plasma physics,” *Plasma Physics and Controlled Fusion* **41**, A747–A755 (1999).
- ⁴⁵T. A. Bechtel, *Stellarator Beta Limits with Extended MHD Modeling Using Nimrod*, Ph.D. thesis (2021), copyright - Database copyright ProQuest LLC; ProQuest does not claim copyright in the individual underlying works; <https://www.proquest.com/dissertations-theses/stellarator-beta-limits-with-extended-mhd/docview/2518726446/se-2?accountid=8330>.
- ⁴⁶Y. Todo and T. Sato, “Linear and nonlinear particle-magnetohydrodynamic simulations of the toroidal alfvén eigenmode,” *Physics of Plasmas* **5**, 1321–1327 (1998), <https://doi.org/10.1063/1.872791>.
- ⁴⁷S. C. Jardin, N. Ferraro, J. Breslau, and J. Chen, “Multiple timescale calculations of sawteeth and other global macroscopic dynamics of tokamak plasmas,” *Computational Science and Discovery* **5**, 014002 (2012).
- ⁴⁸Y. Zhou, N. Ferraro, S. Jardin, and H. Strauss, “Approach to nonlinear magnetohydrodynamic simulations in stellarator geometry,” *Nuclear Fusion* **61**, 086015 (2021).
- ⁴⁹G. Huysmans and O. Czarny, “MHD stability in x-point geometry: simulation of ELMs,” *Nuclear Fusion* **47**, 659–666 (2007).
- ⁵⁰N. Nikulsin, M. Hoelzl, A. Zocco, K. Lackner, and S. Günter, “A three-dimensional reduced mhd model consistent with full mhd,” *Physics of Plasmas* **26**, 102109 (2019), <https://doi.org/10.1063/1.5122013>.
- ⁵¹Z. S. Qu, D. Pfefferlé, S. R. Hudson, A. Baillo, A. Kumar, R. L. Dewar, and M. J. Hole, “Coordinate parameterisation and spectral method optimisation for beltrami field solver in stellarator geometry,” *Plasma Physics and Controlled Fusion* **62**, 124004 (2020).
- ⁵²R. Dewar and S. Hudson, “Stellarator symmetry,” *Physica D: Nonlinear Phenomena* **112**, 275 – 280 (1998), proceedings of the Workshop on Time-Reversal Symmetry in Dynamical Systems.
- ⁵³L. G. Leal, *Advanced transport phenomena : fluid mechanics and convective transport processes* (Cambridge ; New York : Cambridge University Press, 2007).
- ⁵⁴G. O. Spies, D. Lortz, and R. Kaiser, “Relaxed plasma-vacuum systems,” *Physics of Plasmas* **8**, 3652–3663 (2001), <https://doi.org/10.1063/1.1383286>.
- ⁵⁵R. L. Dewar and Z. S. Qu, “Relaxed magnetohydrodynamics with ideal ohm’s law constraint,” (2021), arXiv:2106.12348 [physics.plasm-ph].
- ⁵⁶I. B. Bernstein, E. A. Frieman, M. D. Kruskal, and R. M. Kulsrud, “An energy principle for hydromagnetic stability problems,” *Proceedings of the Royal Society of London. Series A, Mathematical and Physical Sciences* **244**, 17–40 (1958).
- ⁵⁷A. B. Mikhailovskii, G. T. Huysmans, W. O. Kerner, and S. d Sharapov, “Optimization of computational mhd normal-mode analysis for tokamaks,” *Plasma Physics Reports* **23**, 844–857 (1997).
- ⁵⁸G. Huysmans, J. Goedbloed, and W. Kerner, “Isoparametric bicubic hermite elements for solution of the grad-shafranov equation,” *International Journal of Modern Physics C* **02**, 371–376 (1991).
- ⁵⁹C. Schwab, “Ideal magnetohydrodynamics: Global mode analysis of three-dimensional plasma configurations,” *Physics of Fluids B: Plasma Physics* **5**, 3195–3206 (1993), <https://doi.org/10.1063/1.860656>.
- ⁶⁰C. Nührenberg, “Global ideal magnetohydrodynamic stability analysis for the configurational space of wendelstein 7-x,” *Physics of Plasmas* **3**, 2401–2410 (1996), <https://doi.org/10.1063/1.871924>.
- ⁶¹D. V. Anderson, W. A. Cooper, R. Gruber, S. Merazzi, and U. Schwenn, “Terpsichore: A three-dimensional ideal magnetohydrodynamic stability program,” in *Scientific Computing on Supercomputers II*, edited by J. T. Devreese and P. E. Van Camp (Springer US, Boston, MA, 1990) pp. 159–174.
- ⁶²E. Strumberger and S. Günter, “CASTOR3d: linear stability studies for 2d and 3d tokamak equilibria,” *Nuclear Fusion* **57**, 016032 (2016).
- ⁶³M. Drevlak, C. Beidler, J. Geiger, P. Helander, and Y. Turkin, “Optimisation of stellarator equilibria with ROSE,” *Nuclear Fusion* **59**, 016010 (2018).
- ⁶⁴M. N. Bussac, R. Pellat, D. Edery, and J. L. Soule, “Internal kink modes in toroidal plasmas with circular cross sections,” *Phys. Rev. Lett.* **35**, 1638–1641 (1975).
- ⁶⁵A. B. Mikhailovskii, G. T. A. Huysmans, W. O. K. Kerner, and S. E. Sharapov, “Optimization of computational MHD normal-mode analysis for tokamaks,” *Plasma Physics Reports* **23**, 844–857 (1997).
- ⁶⁶S. Yoshikawa, “Toroidal equilibrium of current-carrying plasmas,” *The Physics of Fluids* **17**, 178–180 (1974), <https://aip.scitation.org/doi/pdf/10.1063/1.1694584>.
- ⁶⁷A. H. Glasser, J. M. Greene, and J. L. Johnson, “Resistive instabilities in a tokamak,” *The Physics of Fluids* **19**, 567–574 (1976), <https://aip.scitation.org/doi/pdf/10.1063/1.861490>.
- ⁶⁸J. Manickam, N. Pomphrey, and A. Todd, “Ideal mhd stability properties of pressure driven modes in low shear tokamaks,” *Nuclear Fusion - NUCL FUSION* **27**, 1461–1472 (1987).
- ⁶⁹R. de la Llave, “A tutorial on kam theory,” in *Smooth ergodic theory and its applications* (Seattle, WA, 1999), Proc. Sympos. Pure Math., Vol. 69 (Amer. Math. Soc., Providence, RI, 2001) pp. 175–292.
- ⁷⁰A. I. Khinchin, *Continued fractions*, Vol. 525 (P. Noordhoff, 1963).
- ⁷¹A. D. Bruno, “The analytic form of differential equations,” *Trans. Moscow Math. Soc.* **25**, 131–288 (1971).
- ⁷²G. R. Dennis, S. R. Hudson, R. L. Dewar, and M. J. Hole, “The infinite interface limit of multiple-region relaxed magnetohydrodynamics,” *Physics of Plasmas* **20**, 032509 (2013), <https://doi.org/10.1063/1.4795739>.
- ⁷³R. L. Dewar, “Ballooning-mode Schrödinger equation revisited,” in *Proceedings of the 3rd Australia-Japan Workshop on Plasma Theory and Computation* (Robertson, NSW, 15–17 Nov. 1995), edited by S. A. Dettrick and H. J. Gardner, The Australian National University (The Australian National University, Canberra ACT 2601, Australia, 1996) pp. 21–25, ISBN 0 7315 2450 0.

- ⁷⁴R. Sanchez, S. Hirshman, J. Whitson, and A. Ware, “Cobra: An optimized code for fast analysis of ideal ballooning stability of three-dimensional magnetic equilibria,” *Journal of Computational Physics* **161**, 576–588 (2000).
- ⁷⁵K. Aleynikova, S. R. Hudson, P. Helander, A. Kumar, J. Geiger, M. Hirsch, J. Loizu, C. Nührenberg, K. Rahbarnia, Z. Qu, Y. Gao, H. Thomsen, Y. Turkin, and M. Zanini, “Model for current drive induced crash cycles in w7-x,” *Nuclear Fusion* (2021).
- ⁷⁶D. P. Brennan, E. J. Strait, A. D. Turnbull, M. S. Chu, R. J. La Haye, T. C. Luce, T. S. Taylor, S. Kruger, and A. Pletzer, “Tearing mode stability studies near ideal stability boundaries in diii-d,” *Physics of Plasmas* **9**, 2998–3006 (2002), <https://doi.org/10.1063/1.1481504>.
- ⁷⁷S. A. Henneberg, S. R. Hudson, D. Pfefferlé, and P. Helander, “Combined plasma–coil optimization algorithms,” *Journal of Plasma Physics* **87**, 905870226 (2021).

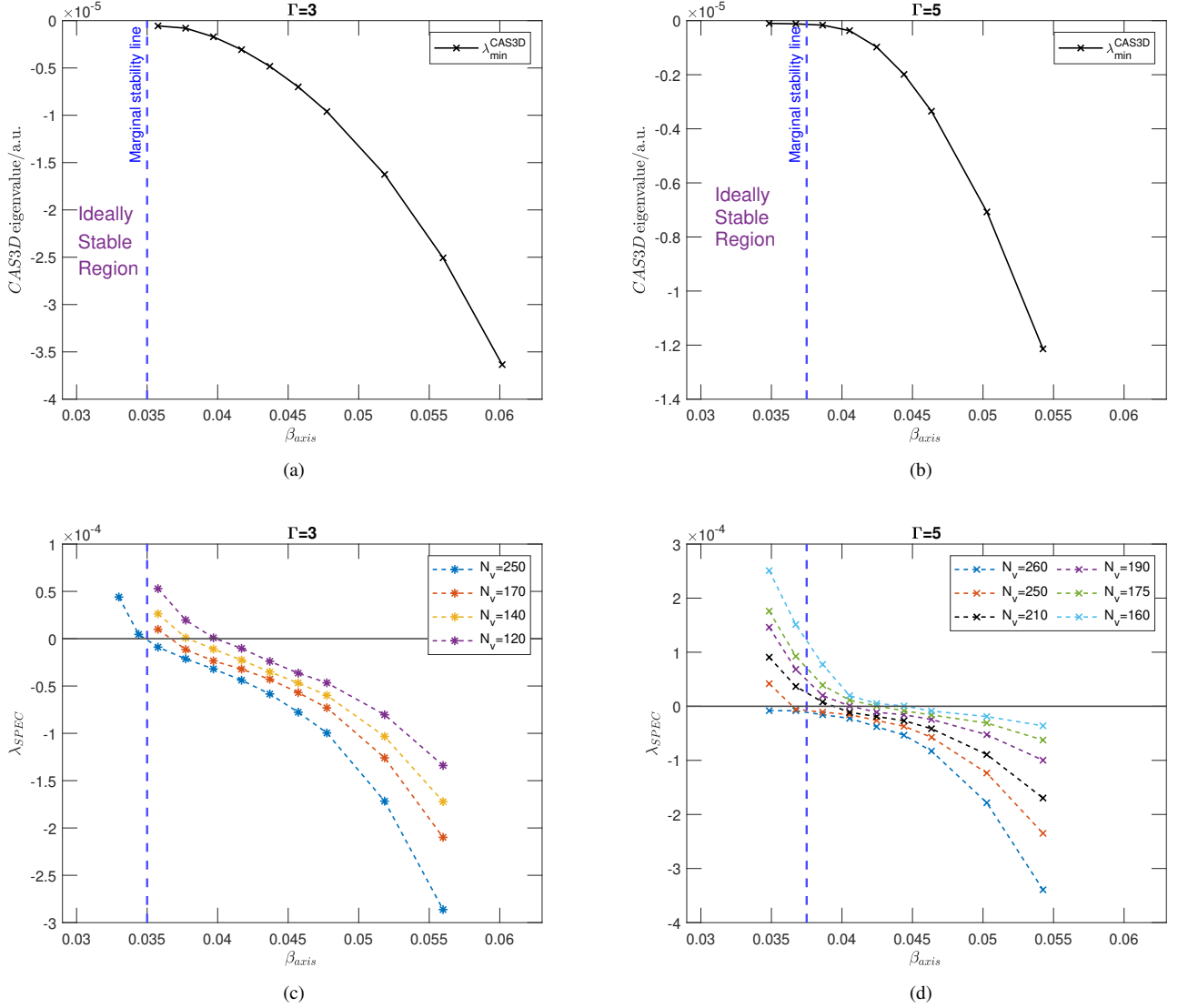


FIG. 7: (a), (b) - ideal MHD eigenvalues λ_{min}^{CAS3D} given by the CAS3D code for a scan over β_{axis} for profile parameter $\Gamma = 3$ and $\Gamma = 5$. The actual size of the CAS3D eigenvalues depends on the kinetic energy normalization, in which the equilibrium number density appears. Note that the blue dashed line on each plots denotes approximated marginal stability limit, which is near $\beta_{axis} \approx 0.035$ for $\Gamma = 3$ and $\beta_{axis} \approx 0.0375$ for $\Gamma = 5$; (c), (d) - the SPEC eigenvalues λ_{SPEC} as a function of β_{axis} for our profile parameter scan $\Gamma = 3$ and $\Gamma = 5$;

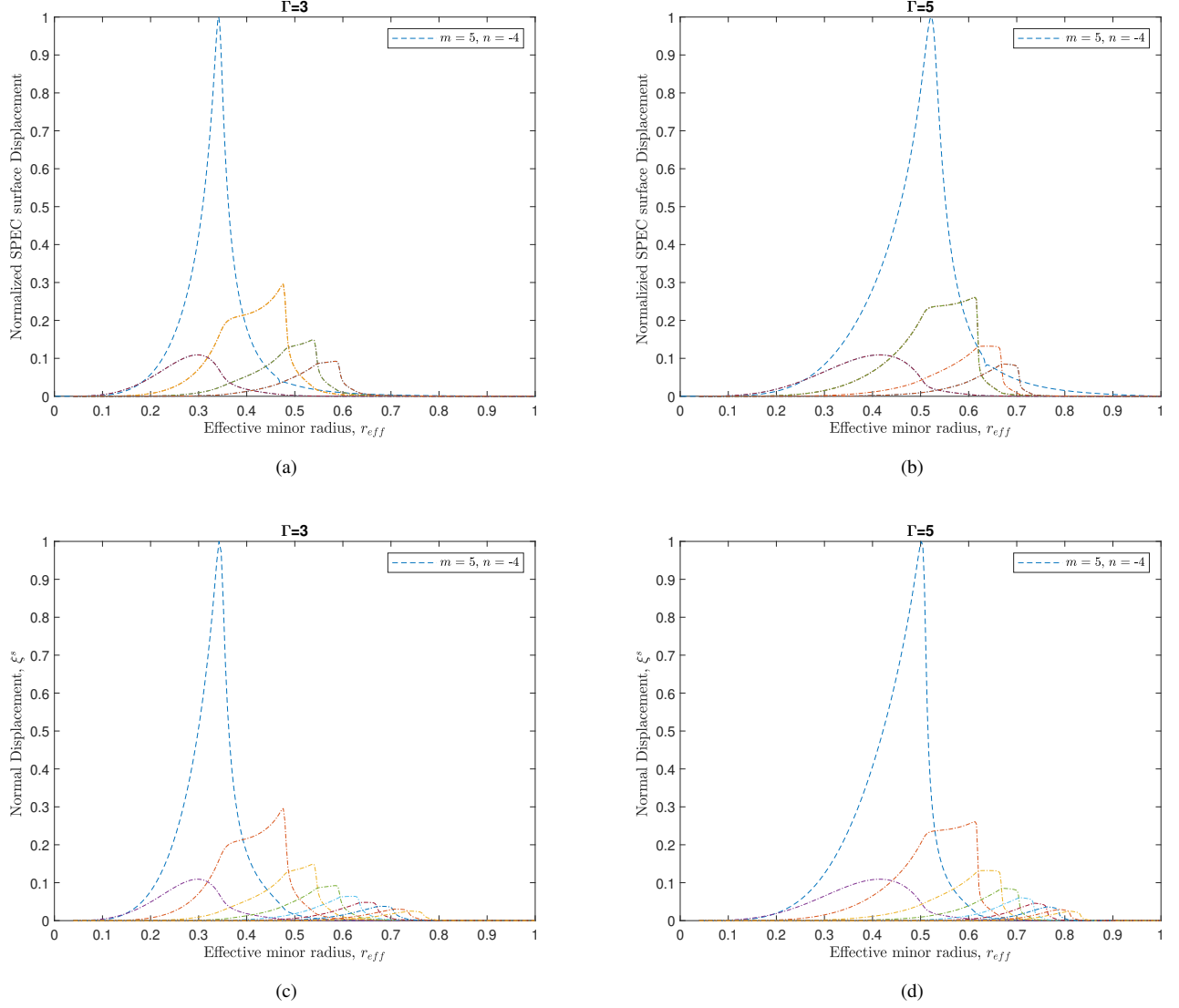


FIG. 8: Plot of : the normalized Fourier amplitudes of eigenmode structure versus r_{eff} computed with SPEC at $\beta_{axis} = 0.038718$ (subframe (a) for $\Gamma = 3$ with $N_v = 250$) and $\beta_{axis} = 0.041502$ (subframe (b) for $\Gamma = 5$ with $N_v = 260$); the radial eigenmode structure (normal component of the ideal MHD displacement vector) versus r_{eff} obtained from CAS3D runs at $\beta_{axis} = 0.038718$ (subframe (c) for $\Gamma = 3$) and $\beta_{axis} = 0.041502$ (subframe (d) for $\Gamma = 5$). A constant mass density was used in the kinetic energy normalization of CAS3D. Here, the $r_{eff} \propto \sqrt{s}$ for the normalized toroidal flux label, s .

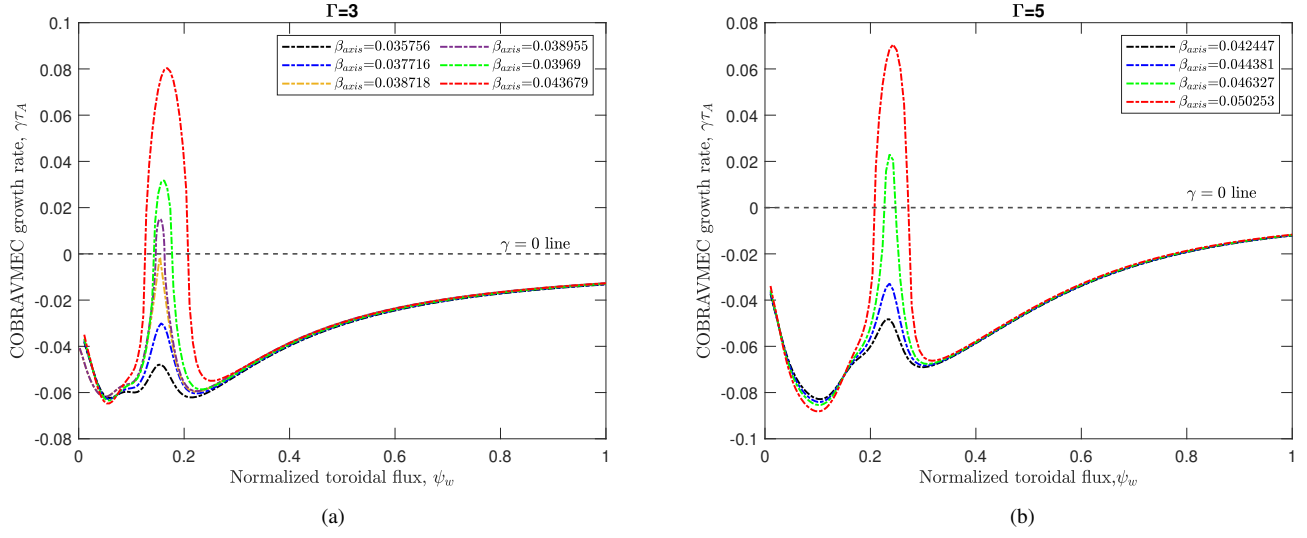


FIG. 9: The radial profiles of COBRAVMEC ballooning growth rates ($\theta = 0, \alpha = 0$) of the most unstable modes, normalized to Alfvén timescale τ_A , vs. the normalized toroidal flux ψ_w when (a) $\Gamma = 3$ and (b) $\Gamma = 5$. The solid black horizontal line denotes the marginal stability.

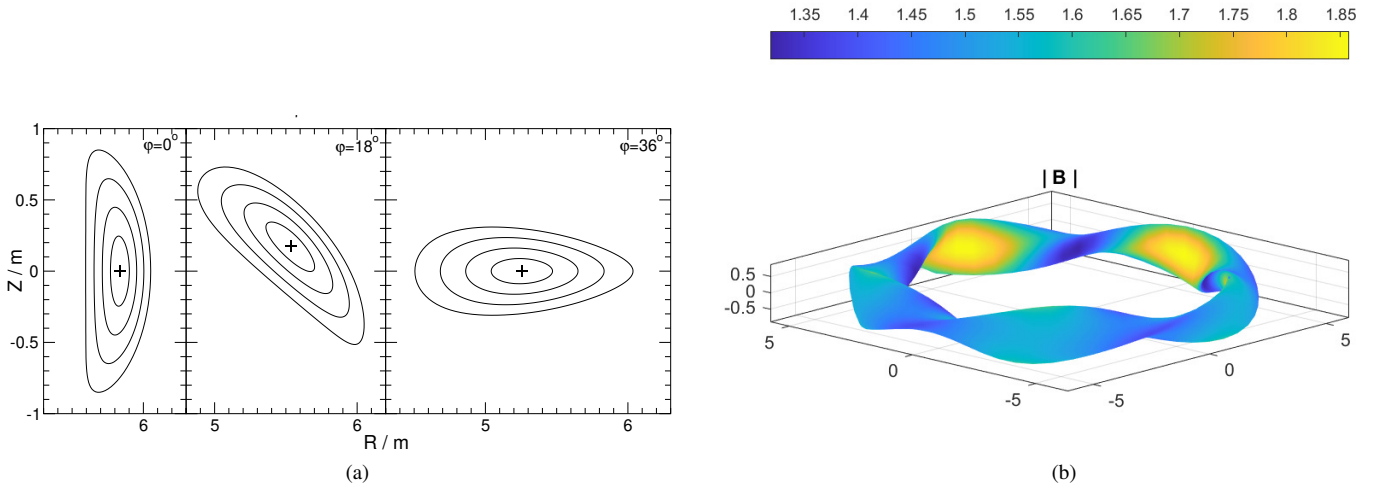


FIG. 10: a) Meridional cuts at the beginning (left), a quarter (middle) and half (right) of one of the five field periods ($N_p = 5$) of the stellarator configuration; b) the three-dimensional plot of the stellarator boundary. Colours indicate the magnetic field strength in Tesla (T).

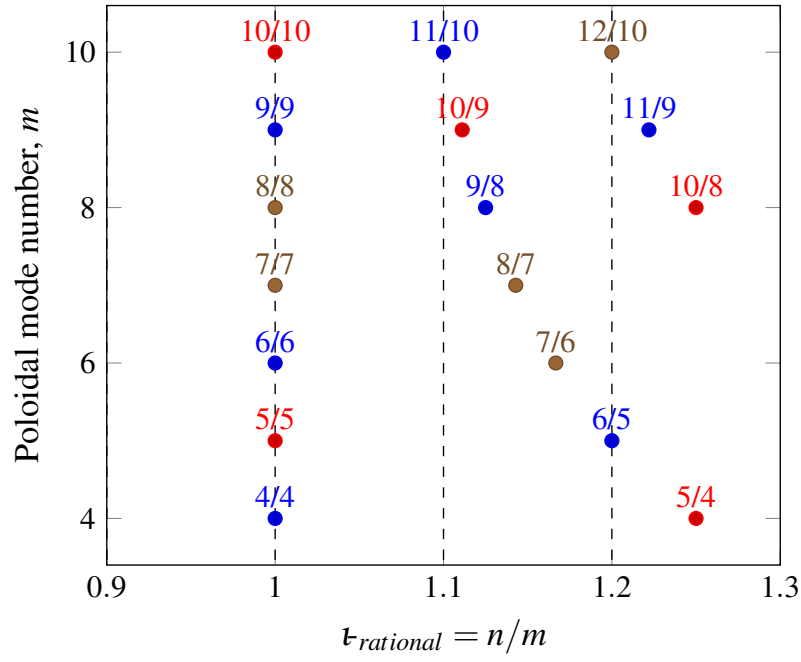
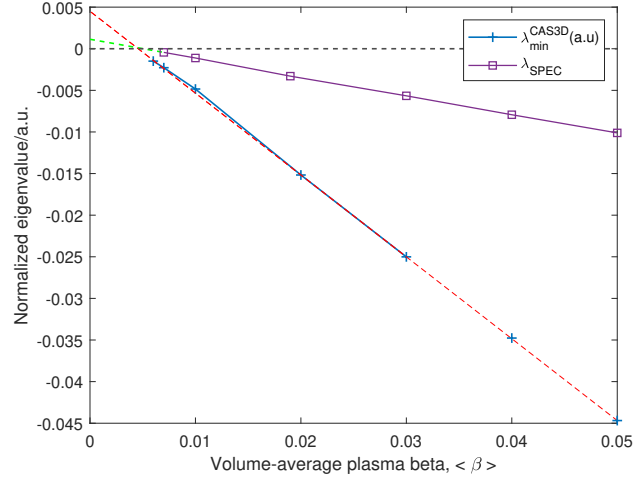
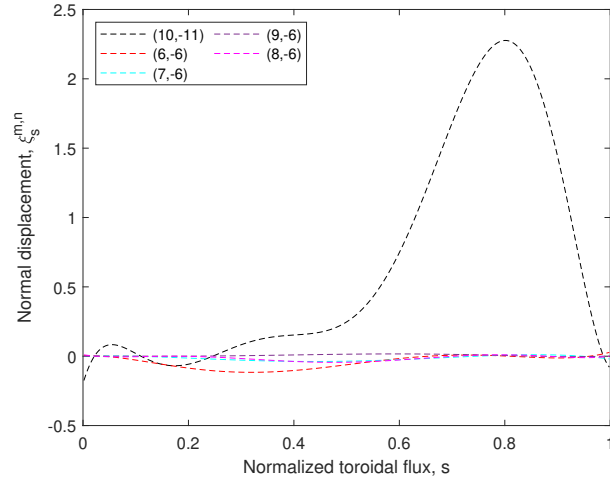


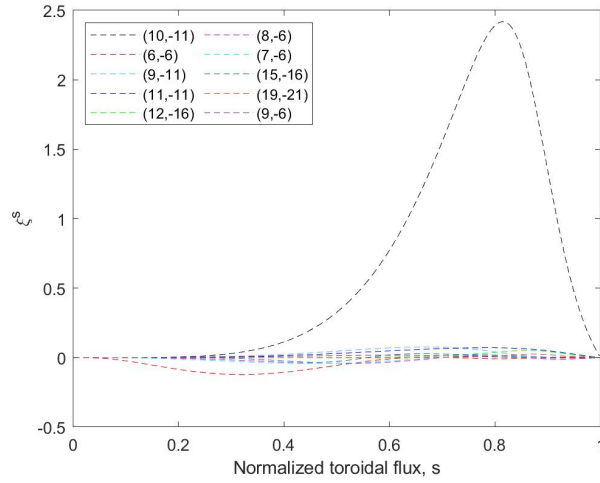
FIG. 11: Rational values $\iota_{rational} = n/m$ (in the rotational transform), located in the $(\iota_{rational}, m)$ -plane, with m and n being poloidal and toroidal Fourier indices. The different shadings/dots reflects the 3 mode families of our five field period stellarator configuration: red denotes the $N = 0$ family, blue denotes the $N = 1$ family, and light brown denotes the $N = 2$ family. This plots shows a subset of the (ι_R, m) -plot from Nührenberg⁶⁰.



(a)

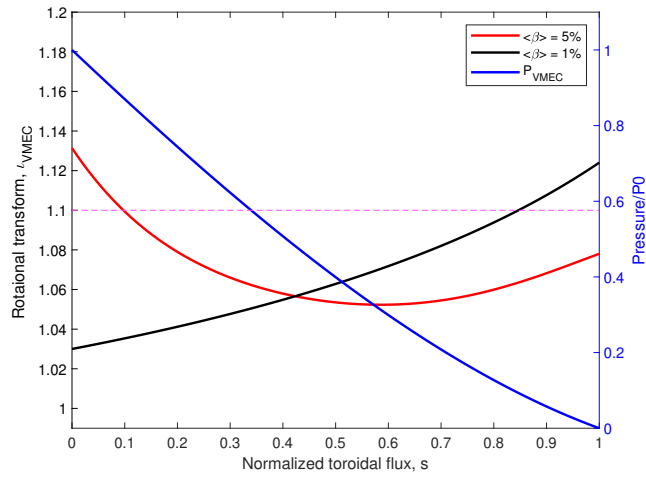


(b)

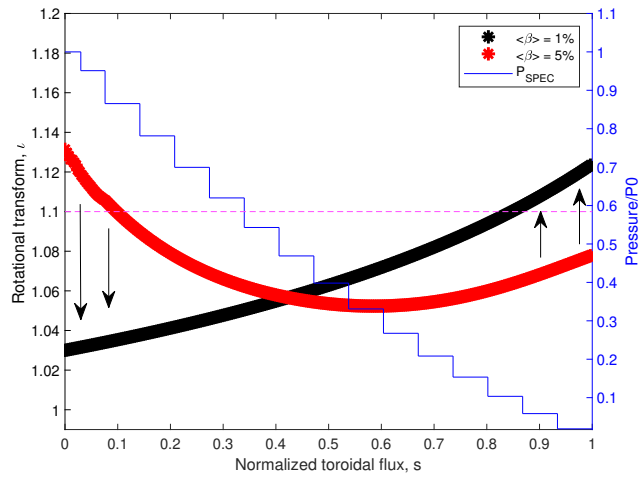


(c)

FIG. 12: Plot of: a) the λ_{SPEC} and λ_{min}^{CAS3D} versus volume-averaged beta $\langle \beta \rangle$ scan. Eigenvalues obtained from both SPEC and CAS3D runs are linearly extrapolated to approximate the marginal stability limit, $\langle \beta \rangle \approx 0.0051$ (the $\langle \beta \rangle$ value at the intersection of extrapolated green and red lines); b) the radial behaviour of dominant normal displacement $\xi_s^{m,n}$ Fourier coefficient (of SPEC) for the mode in the unstable values of $\langle \beta \rangle = 0.01$; c) the radial eigenmode structure (normal component of the ideal MHD displacement vector) as a function of normalized toroidal flux (denoted as s), obtained from CAS3D calculations for unstable beta value, $\langle \beta \rangle = 0.01$. A non-uniform mass density was used in the kinetic energy normalization of CAS3D.



(a)



(b)

FIG. 13: Plot of: a) VMEC iota profiles; b) SPEC iota profiles versus normalized toroidal flux, s . The dashed line indicates the location of low order rational $\iota = 11/10$. In each of the plots, the normalized pressure profile versus s is shown in blue curve. The change of ι with $\langle \beta \rangle$ is indicated by black arrows.

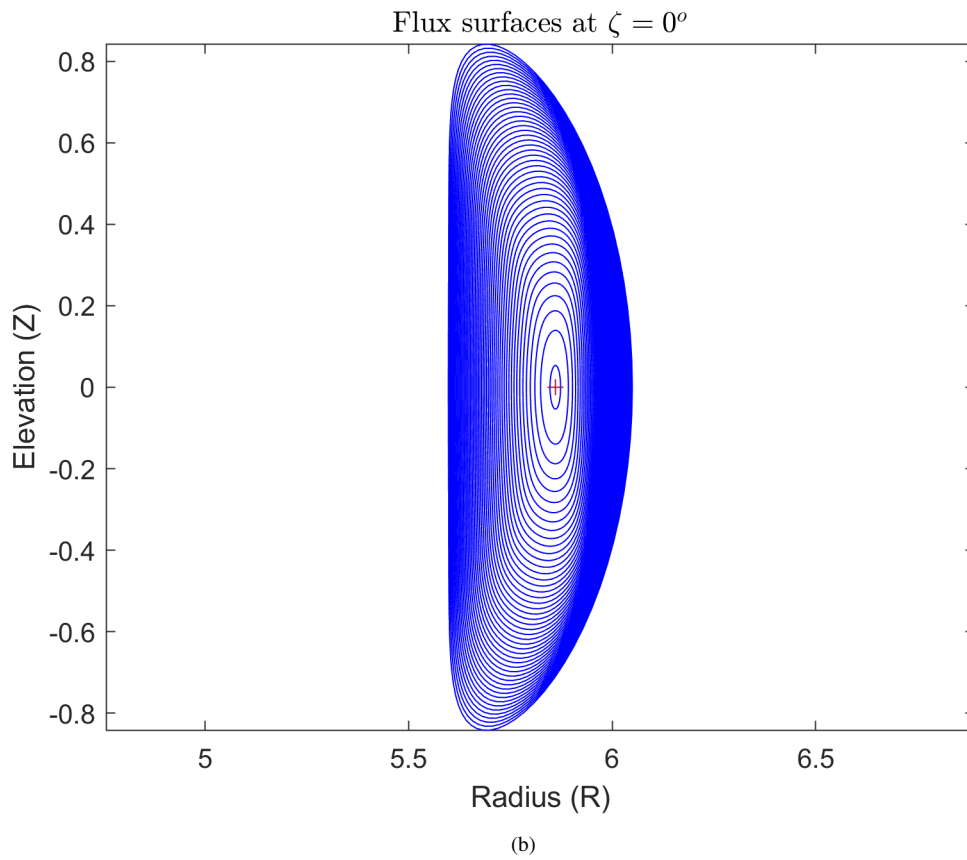
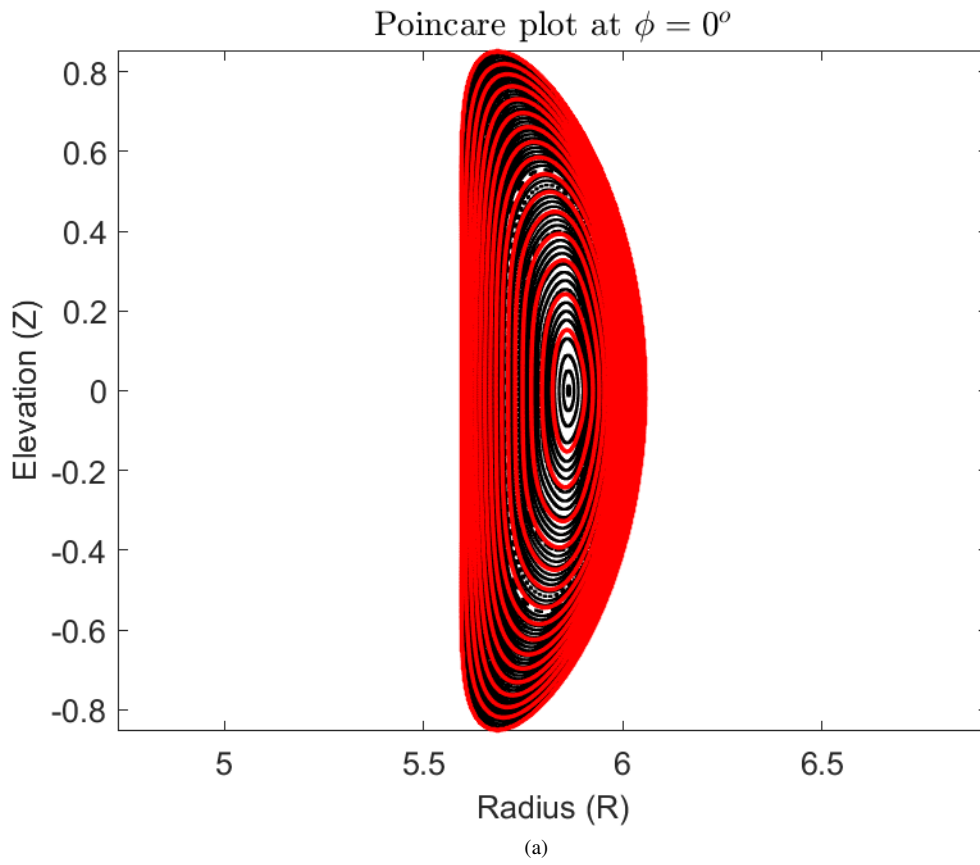


FIG. 14: Plot of: a) the Poincaré cross-section at $\phi = 0^\circ$ of MRxMHD equilibrium obtained with SPEC at $\langle\beta\rangle = 5\%$. The red solid contours indicates the position of the interfaces; b) the VMEC equilibrium with nested flux surfaces at $\langle\beta\rangle = 5\%$.